SLAC TRANS 49

Eichmessungen mit Faradaykäfig, Kalorimeter, Quantameter und Sekundäremissionsquantameter am externen Elektronenstrahl 1 Gev bis 5 Gev (Calibration measurements by means of a Faraday cage, calorimeter, quantameter, and secondary emission quantameter on an external electron beam in the energy range of 1-5 Gev) by A. Ladage and H. Pingel. DESY Report 65/12 (August 1965) 75 pp. Translated from the German (November 1966) by J.M. Silberstein.

TRANSLATED FOR

STANFORD LINEAR ACCELERATOR CENTER

****

CALIBRATION MEASUREMENTS BY MEANS OF A FARADAY CAGE, CALORIMETER, QUANTAMETER, AND SECONDARY EMISSION QUANTAMETER ON AN EXTERNAL ELECTRON BEAM IN THE ENERGY RANGE OF 1-5 GEV

A. Ladage

H. Pingel

C o n t e n t s

A b s t r a c t

Calibration measurements have been done on the external electron beam at DESY in the energy region 1.5 Gev to 5 Gev with a Faraday cage, a calorimeter, several gas-filled quantameters, and a secondary emission quantameter, using a thin secondary emission monitor of 2×10^{-2} radiation length as an intermediate standard.

The responce of the monitors was investigated over a wide range of intensities and energies, and for various beam positions across the aperture. Plateaus were measured, and short- and long-term stability was checked.

Our data indicate that the Faraday cage measures the charge of the electron beam with an error of 0.3% up to 5 Gev. An intercalibration between the Faraday cage and the calorimeter at 3 Gev showed agreement within $\pm$ 0.7% between the measured charge of the Faraday cage and the charge derived from measuring the total energy of the electron beam in the calorimeter.

Four gas-filled quantameters were compared and calibrated against the Faraday cage. All quantameters are made of copper; one of them has copper surfaces, the others have gold plated surfaces 4 μ thick. In all other respects they are identical. The gold plating permits the use of the quantameters as secondary emission quantameters under clean surface conditions after evacuation.

The calibration constant of the quantameter with copper surface has very nearly the theoretical value of 4.9×10^{18} Mev$\cdot$coul^{-1} calculated from the work of Wilson[1]. The measured constant is 4.75×10^{18} Mev$\cdot$coul^{-1}.

Surprisingly, the other three quantameters with gold-plated surfaces show 26% more current than the quantameter with the copper surface. The calibration constant is about 3.6×10^{13} Mev.coul^{-1} within $\pm$ 2.5% for the three different quantameters mentioned. No energy dependence of the calibration constant was found in the region from 1.5 to 5 Gev.

The unexpected dependence of the calibration constant of the gas-filled quantameters on the type of surface suggests that the deviations between the measured and the calculated calibration constants found at other laboratories[10], might be due to varying surface conditions.

Data are also given for the calibration constant of the secondary emission quantameter. The main advantage over the gas-filled quantameter is the absence of saturation effects at high intensities. Therefore, we are planning to use the secondary emission quantameter with all high-intensity γ-ray beams.

1. Introduction

Since March 196[illegible] external γ-rays with an intensity of approximately 5×10^8 of effective quanta per pulse have been available at DESY for experimental purposes.

Gas-filled quantameters[1] are used as radiation monitors for the measurement of the intensity of these external beams; their calibration constants were determined by calculation.

The intention was to change some of these quantameters for high-vacuum operation and use them as secondary-emission quantameters for higher intensities. With a view to obtaining specific surface conditions the copper surfaces of the plate assembly which absorbs the shower were gold-plated in these quantameters (type D3).

Comparison measurements of the two types of quantameters have shown that the calibration constant of the meter with gold-plated plates was 26% smaller than the theoretical[1] constant of the two types (the same geometry) equal to 4.9×10^{18} Mev.coul^{-1}. This difference in the constant of the quantameters type 3 was confirmed by two-at-a-time spectrometer measurements, with an accuracy of 5%.

There is as yet no quantitative explanation of the discovered surface effect, which is not considered in Wilson's theory[1].

In order to establish this effect more accurately we undertook an

absolute calibration of the quantameter on the first external beam in which a Faraday cage and a calorimeter served as reference standards. The external electron beam required for this purpose was available, beginning from May 1965, with a maximum intensity of about 5×10^{10} electrons per pulse in the energy range of 1.5-5 Gev.

The calibration experiments carried out in June and July 1965 have settled the following problems:

1. Checking and determining the absolute accuracy of a Faraday cage (3.1),
2. Checking and calibrating a thin secondary-emission monitor to be used as an intermediate standard in all measurements (3.1),
3. Checking a calorimeter and comparing this independent standard with the Faraday cage (3.2),
4. Calibrating a gas-filled quantameter to be used as the standard for γ-rays (3.4),
5. Checking and calibrating a secondary-emission quantameter to be used as the standard for γ and beta rays of high intensity (3.5).

Within the limits of the time spent on measurements, all the above-listed instruments were studied for their dependence on the energy and the intensity of the electron beam.

2. Construction of the monitors used

2.1. Faraday cage

2.1.1. Construction

Figure 1 shows the cross-section of the Faraday cage built for 7.5 Gev. The electron beam enters the vacuum chamber penetrating through a spring bronze foil 10^{-2} radiation lengths thick and 15 cm in diameter. A vacuum of 5×10^{-7} torr is produced by an ion getter pump. Behind the entrance foil, a permanent magnet of 7000 gauss.cm deflects the generated secondary electrons towards the chamber walls. Electrons with energy below 3 Mev do not reach the radiation absorber. Errors in the charge measurements, caused by the secondary electrons from the foil itself, are expected to be less than 10^{-3} since the main body of the secondary electrons have only an energy below 50 ev. This is shown, for instance, by plateau measurements on the 6BM in Figure 12.

The lead absorber is placed on aluminum oxide insulators which have an insulation resistance of 10^{14} ohm. Its length is equal to 200 radiation lengths; 120 radiation lengths correspond to the radiation entrance channel which has a diameter of 15 cm. The absorber diameter is 150 radiation lengths.

In order to reduce back-scatter, the electron beam meets a 5 cm thick carbon layer before it hits the lead. Secondary electrons are pre-

vented from escaping from the absorber by another permanent magnet (specification as above). Since the electron beam surrenders the major part of its energy in the first 10 radiation lengths, lead is replaced in this part by tungsten because lead might start melting.

The lead absorber is situated in aluminum housing. This reduces the generation of secondary electrons by the photoelectric and Compton effects. The vacuum chamber is also made of aluminum, for the same reason.

A potential of up to 3 kv can be applied to the aluminum mesh which surrounds the absorber, when the charge loss is measured. As compared to the other equivalent method in which the potential is applied directly to the lead absorber, our method has the advantage in that the instruments measuring the cage current remain grounded, and the charge loss of the cage can always be checked in operation in a simple manner.

2.1.2. Dimensions of the absorber

With a view to determining the absorber dimensions, Brown and Tautfest's computations[2] were compared with Nagel's Monte-Carlo calculations[3] which were carried out for energies between 100 and 1000 Mev. In the meantime,

U. Völkel of DESY[4] has extended these calculations up to 6 Gev. In the Monte-Carlo computations electrons down to 1 Mev and photons down to 0.25 Mev were considered. Nagel's paper also contains extrapolation formulas for the position and height of the shower maximum, data relating to the fall of intensity after the shower maximum, and information about back-scattering. When it is postulated that, say, only 10^{-3} of the primary electrons may escape from the absorber, the calculations of Brown and Tautfest and those of Nagel agree well in their determination of the absorber length.

Since Nagel's data are based on the electron cut-off energy of 1 Mev, Brown and Tautfest's calculations should really produce greater dimensions, because of the low-energy electrons. This is also shown by the reduction of the photon intensity which occurs considerably slower in Nagel's calculations than in those of Brown and Tautfest, and also slower than would correspond to the minimum absorption factor. Photons with energies below 0.25 Mev might therefore be present in even greater numbers, and hence low-energy electrons as well.

However, their travel range is very small and the above discussed

computations should provide a good guidance to the absorber dimensions, if only they are based on the reduction not of electrons but of photons.

It was intended to have an accuracy of about 1×10^{-3} in the charge measurements of the electron beam at 7.5 Gev. This specification produced the length and the diameter of the absorber using Nagel's extrapolating formulas.

Nagel also gave some data of the back-scattering effect. When these data are extrapolated to 7.5 Gev, it is found that about eight times as many photons with an energy greater than 0.25 Mev escape from the absorber as the primary electrons which enter it. Above 10 Mev, there is still about 5%. In the angular range of 170°-180° there is still about 20% of photons with energies of 0.25-5 Mev.

For the above reason, the entrance channel of the absorber was made so long that the photons deviating backwards from the entrance aperture make about 15% of the total. Only in the area of the entrance foil and the permanent magnet do they meet dispersing matter, and the effect of secondary electrons produced in this manner on the accuracy of the charge

measurement must therefore be negligible.

2.2. Secondary emission monitor (SEM)

The secondary emission monitor is used as an intermediate standard for checking and calibrating the Faraday cage, the calorimeter, and the quantameters. Since it is placed before other instruments in the path of the beam, it must be as thin as possible to reduce the scatter.

Figure 2 shows a cross-section of the secondary emission monitor. The vacuum chamber is closed by the beam entrance and exit windows made of spring bronze, each 10^{-2} radiation length thick and with a diameter of 20 cm. A vacuum of 10^{-7} torr is produced by an ion getter pump.

There are 17 aluminum foils, each 6×10^{-3} mm or about 10^{-4} radiation length thick, connected alternately to the supply voltage and to the collector.

Using optical diaphragms and gratings, the ion current from the pump was reduced to 10^{-13} a. Currents of 10^{-11} a can therefore be reliably measured by the secondary emitter monitor. Generally speaking, the actual measurement range was between 10^{-7} and 10^{-10} a.

2.3. Calorimeter (KM)

In addition to the Faraday cage, a calorimeter was also used for absolute measurements; its cross-section is shown in Figure 3. A lead cylinder 18 cm in diameter and 20 cm long absorbs about 99.7% of the electron beam energy at 6 Gev. This figure results from the Monte-Carlo computations of U. Völkel[4].

The absorber is thermally insulated by a 10 cm layer of polystyrene foam (Styropor) which completely surrounds it. The heat loss corresponds to a temperature drop of 0.05°C per 10 minutes at 30°C. The temperature of the absorber is measured by a platinum resistance thermometer.

The calorimeter is calibrated using a heater element cast into lead. The electrical energy was supplied by a current-stabilized d-c supply and measured with an accuracy of about 0.2% by digital voltmeters and DESY integrators. The power at which the calibration was performed corresponded to the electron beam with an available power of 100-200 w. A heating or irradiation period of 10 to 20 minutes was required to raise the temperature by 10°C.

The heat loss through the insulation may be neglected in this method because the heating and irradiating powers are equal.

The calorimeter has a cooling coil and can be cooled down within approximately 10 minutes from the end of the measurement.

2.4. D S S Y quantameter (QM, SSQ)

The DESY quantameter is a gas-filled instrument based on the principle proposed by R.R. Wilson[1].

The plate assembly which absorbs the shower energy is in Wilson's quantameter composed of two setsof interlaced copper plates, all of the same thickness; one set - every alternate plate - carries an auxiliary potential required for the gas discharge in the quantameter, whereas the other set - the plates interlaced between those to which the voltage is applied - is well insulated (Figure 4). The second set serves as a collector for the measured gas discharge current which is proportional to the shower energy.

Since there are stringent requirements regarding the electrical insulation (about 10^{12} ohm), the collector set is also well insulated ther-

mally, and is therefore able to pass, practically only by radiation, one half of the shower energy which it absorbs to the voltage-carrying set of plates. H ating of the collector plates is therefore excessive at the higher beam intensities, and the gas discharge gap varies more than the permissible mechanical tolerance.

For this reason, following the idea of W. Kern, nearly all the energy of the shower is absorbed in the DESY quantameter (type D1 and D3) by a set of twelve 14.90 mm thick electrolytic copper plates connected to the source of the auxiliary potential, while 0.10 mm thick copper foils are employed as the collector and absorb only 1/150 part of the total shower energy (Figure 4). The total thickness of the plate assembly was chosen for the DESY maximum energy of 7.5 Gev on the basis of the "linear" shower theory[5].

The length of the gas discharge gaps changes, because of the Simpson integration over the shower curve, in the ratio of 2 : 1 and is 2 x 1.50 mm or 2 x 0.75 mm. The width of the correcting gap at the end of the plate assembly, which allows for the theoretical exponential fall of

the shower curve, is 2 x 3.575 mm and is equal to the equivalent width of the radial correcting gap.

DESY quantameters are filled with the gas mixture suggested by Wilson (95% Ar and 5% CO_2) in which argon has 7 ppm of impurities and CO_2 20 ppm. Because of the saturation of the gas discharge, the gas-filled quantameter can be used only at a low radiation intensity.

Unlike the gas-filled type, the secondary-emission quantameter proposed by H. Fischer and C. Schaerf[6] is independent of the intensity in the range known at present; however, this monitor must be calibrated by means of another standard instrument (e.g. a Faraday cage, a gas-filled quantameter, or a calorimeter).

The DESY quantameter (D3) represents a combination of the gas-filled and the secondary-emission types. It can be used at low beam intensities as a gas-filled quantameter with a high "current magnification" of the gas discharge. On the other hand, at higher beam intensities it is evacuated by means of its ion getter pump to a good vacuum ($p < 10^{-6}$ torr) and is then used as a secondary emission quantameter.

It is well known[7,8] that the secondary emission of a metal surface depends greatly on the latter's state (e.g. oxide film, etc.); good long-term stability can be achieved only with a superior surface finish or by the use of a suitable material. (The plate assembly of the secondary-emission quantameter developed in Stanford is for this reason made of silver.)

For the same reason, the surfaces of the plates and foils in the DESY quantameters are electrolytically gold-plated. The plating is about 4 μ thick.

The insulation resistance between the collector and the guard ring in the DESY quantameters is greater than 10^{12} ohm, and it is possible to measure reliably currents down to 10^{-10} a.

2.5. Current meters and integrators

An integrator developed at DESY is used for measuring currents greater than a few nanoamps.

The measuring circuit of the DESY integrator consists essentially of two commercially available, chopper-stabilized, operational amplifiers (Philbrick USA 3) connected in series. The first amplifier has negative

feedback via a high-resistance circuit and acts as an impedance changer and current meter, while the second amplifier integrates the current on a capacitor. The use of a bias charge principle, which makes it possible to obtain measurements even when the integration capacitor value is not accurately known, and employment of high-precision high-value resistors in the feedback circuit ($\pm$ 0.1%) allowed us to achieve in all current ranges (10^{-8}-10^{-3} a) a long-term calibration stability better than $\pm$ 0.5%.

For the measurement of currents below 10^{-9} a, a vibrating-capacitor electrometer (IDL) is used instead of the first operational amplifier. The values of the feedback resistances which determine the current range can be changed by remote control. Currents can be measured from 10^{-4} to 10^{-12} a. The accuracy is $\pm$ 0.5% in the range of 10^{-4}-10^{-8} a, and $\pm$ 1% in the range of 10^{-9} to 10^{-12} a.

3. Layout of the experimental setup

Figure 5 shows the layout of the experimental setup.

The electron beam is sent out from the synchrotron by means of an ejection system (not shown) and meets the first collimator. The horizontal dispersion of the beam guiding system has a maximum at the point where the

second collimator is located, which limits the defocussing of the beam to $\pm$ 0.5%. The dispersion of the nominal-energy electrons is cancelled by the second deflection magnet. The quadrupoles focus the beam in both planes at the point of location of the Faraday cage (FK) or quantameter (Qu).

The design of the beam-guiding system is such as to permit the measurements in the energy range of 1.5-5.0 Gev.

For an accurate measurement of energy the electron beam is adjusted by the first deflecting magnet in such a manner that it optimally travels through the second collimator and the preceding scintillator (Sz1) which has an aperture at the point that should theoretically be traversed by the beam. Coarse adjustment of the current in the deflecting magnets is carried out by watching the scintillator Sz1 by means of a double mirror (D) and television camera (Fs). Fine adjustment of the current is performed by measuring the current in the insulated second collimator. When the adjustment procedure is finished, the direction of the current in the first deflecting magnet is reversed (its intensity remains the same) and the beam can be then watched through the other half of the double mirror D on a

cross-wire of the second scintillator Sz2.

The two beam trajectories are made symmetrical. When the beam hits the deflecting magnet exactly perpendicularly, and the deflection current remains the same, the same deflection is observed.

The electron-beam energy can be measured by this method with an accuracy of $\pm$ 0.5-1.0%.

There is a further deflecting magnet between the secondary emission monitor (SEM) and the Faraday cage (FK) or quantameter (Qu), which removes γ -quanta from the electron beam.

In addition to the SEM which is used as the intermediate standard in all measurements, a thin gas-filled ionization chamber is also situated in the beam path, which serves as a second independent intermediate standard at lower intensities. Figure 6 illustrates the arrangement of the SEM and the ionization chamber.

Figure 5 shows the Faraday cage ready for measurement at the end of the beam. Together with the quantameter it is set on a trolley which makes it possible to interchange the monitors at will (Figure 7). The

calorimeter, which is employed as an additional comparison standard, can be set on the trolley in front of the quantameter.

4. Measurements

4.1. Faraday cage and secondary emission monitor

The secondary emission monitor (SEM) is used as an intermediate standard for the control and calibration measurements, together with the Faraday cage and the quantameter. The most important points of its specification are stability during the measurement and linearity in the entire intensity range.

4.1.1. Stability of the SEM

The short- and long-term stabilities of the ratio of charges, Q_{FK}/Q_{SEM} are plotted in Figures 10 and 11. It is evident that the secondary emission current increases in the first few minutes of irradiation by about 3%, and then stays constant to $\pm$ 0.5% for several hours. This effect can be explained by a surface change under irradiation[7] since the secondary emission current is composed mainly of electrons with an energy lower than 20 ev.

This is shown by the measurement of the voltage dependence of the SEM (Figure 12). Presumably, the adherent residue of gas is removed by irradiation of the surface[8].

The long-term stability of the SEM is ± 1% over a period of four weeks. During this period, and in the preceding three months, vacuum was maintained at 1×10^{-7} torr by an ion getter pump without ventilation.

Apart from the change in sensitivity in the first 20 minutes after the beginning of exposure, the stability of the SEM is within the limits required for our measurements.

4.1.2. Linearity of the SEM

The dependence on the intensity is illustrated in Figure 13. The measured charge ratio, Q_{FK}/Q_{SEM}, is constant within ± 1% in the range extending from 10^6 to 10^{10} electrons per synchrotron pulse. This result is in agreement with the measurements of other workers[7-10].

4.1.3. Energy dependence of the SEM

Contradictory measurements of the energy dependence of secondary emission monitors have been published[7-11]; there are also discrepancies between these measurements and the theoretical results of Vanhuyse and van de Vijver[12].

Evaluation of the measurement results is thus made more difficult because a possible energy response of the Faraday cage would also affect these results.

Figure 14 shows the ratio of Q_{FK}/Q_{SEM} in the range of 1 to 5 Gev. It is constant to $\pm$ 1% and does not depend on the energy.

This agrees with the measurements of Taulfest and Fechter[9] in the range of 100-250 Mev, but is contradicted by the measurements of de Pagter and Fotino[10]; the latter authors found that the ratio Q_{FK}/Q_{SEM} was reduced by 4.5% in the energy range of 1 to 5 Gev. They pointed out the discrepancy with the theory[12] which predicts a fall of 7.5%.

The measurement results obtained by de Pagter and Fotino for Q_{FK}/Q_{SEM} include also the energy dependence of the Faraday cage which amounts to about 2%. If this factor is eliminated, the energy response of the SEM is reduced to 2.5%, and the discrepancy between this and theoretical dependence becomes even greater.

4.1.4. Charge loss and energy dependence of the Faraday cage

The charge loss in a Faraday cage is evaluated by applying an auxiliary

potential to the lead absorber or by applying various voltages to the mesh which surrounds the lead absorber. Both methods were in use : they are equivalent.

Figures 15 and 16 show the results obtained for 2.9 and 4.6 Gev. The relative loss of electrons in the Faraday cage amounts to $(1.9 \pm 0.9) \times 10^{-3}$ and to $(3.2 \pm 1.5) \times 10^{-3}$. All the measured results of the relative charge loss are plotted in Figure 17 against the electron energy. It is not possible to exclude the possibility of an energy dependence amounting to a few parts per 1000. In the energy range of 1 to 5 Gev the mean value of the relative charge loss is $(2.8 \pm 1.2) \times 10^{-3}$.

Comparison with de Pagter and Fotino's[10] results which indicate a charge loss of about 1.7×10^{-2} leads to a question of where does this fivefold increase of the loss come from. Presumably it is due to a substantially shorter beam input channel (only 50 instead of 120 radiation lengths), because the difference in other dimensions is much smaller.

This is also indicated by the results obtained by Brown and Lautfest[2] on a Faraday cage for 300 Mev. In their case the relative electron loss

is also only a few parts per 1000, and their beam entrance channel is twice as long as the absorber itself. The same Faraday cage was used by Tautfest and Fechter[9] in their measurements of Q_{FK}/Q_{SEM}; in this case as well there is no energy dependence in the range of 100 to 250 Mev, and the above ratio remains constant in this range to about 0.5%. This agrees with our measurements of Q_{FK}/Q_{SEM} in the range of 1-5 Gev (Figure 14).

An additional clue for the evaluation of the charge loss in Faraday cages is provided by the measurement of the mesh current. At 4.8 Gev a positive mesh current was measured, amounting to 1.5×10^{-3} of the cage current; it is, evidently, due to the electron emission of the mesh, stimulated by photons from the absorber. Since both the mesh and the surface of the absorber are made of aluminum, and since the discussion in Section 2.1.2 indicates that the relative number of the photons escaping from the absorber can be greater than one part in thousand only in the case of the photons below 250 kev, all electrons produced in the aluminum have travel ranges much lower than the wire diameter of the mesh (1 mm). Hence

the absorber and the mesh surface can be regarded to a first approximation as similar electron emitters. The relative mesh current of 1.5×10^{-3} parts leads therefore to the conclusion that the charge loss in the absorber is a few parts per thousand; the measurements of the charge loss quoted previously produced a figure of $(2.8 \pm 1.2) \times 10^{-3}$. Thus, the Faraday cage meets the required accuracy of measurement of the charge in the electron beam.

4.1.5. Usable aperture of the Faraday cage

The geometric aperture of the Faraday cage is equal to the internal diameter of the beam entrance channel (15 cm) in the lead absorber. Figure 18 shows the sensitivity of the Faraday cage as a function of the horizontal location of the beam entrance point. This was measured with an electron beam which had a diameter of about 10 mm (Figure 8). Within the area of measurement errors (± 1%) the Faraday cage has the same sensitivity in the entire aperture area. At the edge, the beam meets the magnet rods behind the entrance foil and the cage current falls to a small extent. As the beam distance from the middle point of the cage is increased, the measured

current rises rapidly. The beam hits the flanges of the vacuum chamber and stimulates secondary electrons which penetrate unhindered into the lead absorber.

It is evident that the electron beam can have any shape and position within the geometric aperture, and that this will not affect the accuracy of the measurement.

However, substantial errors may ensue when parts of the beam hit the aperture edge. This has actually occurred once during our measurements because of imperfect beam guidance (see Figure 9); the charge ratio, Q_{FK}/Q_{SEM}, was then 5% greater than normally.

The reason for this was not known at first and the charge loss of the Faraday cage was measured in a search for an explanation (see 4.1.4). There was no plateau up to 3.5 kv on the mesh. The measured charge loss was rising linearly with the mesh voltage, and at 3.5 kv and for 1.5 Gev, amounted to about 1.5%. For the sake of accuracy of the measurement, the beam profile must therefore be kept under control.

4.1.6. Leakage currents in Faraday cage

The major component of these currents is due to ions from the 200-liter ion

pump used. Using optical lenses and a grating, this component was reduced to 2×10^{-12} a, for a vacuum of 6×10^{-7} torr. Since the measurements are generally running at the current level 10^{-9} to 10^{-7} in the cage, this leakage current may be obviously neglected.

The current through the insulation is much smaller and amounts to only $\sim 10^{-16}$ a; such currents result from the measured insulation resistance of 10^{14} ohm and the voltage of 0.01 v applied to the absorber when full deflection of the current meter is reached.

A further leakage current is produced in the connecting cable to the measuring setup, due to stray radiation from the Faraday cage. At 3 Gev the cable current was 3×10^{-5} parts of the beam current.

4.2. Calorimeter

4.2.1. Calibration of the calorimeter

For the calibration purposes the calorimeter was heated electrically and the temperature was recorded every 30 seconds. Figure 19 shows a typical temperature-time graph. In the heating period the temperature rises linearly.

The spacing between the heating element and the thermometer causes an indication delay of about two minutes. Perfect thermal equilibrium is reached only about 20 minutes after the heating is switched off. The temperature fall per unit time, caused by the insulation losses, is then approximately constant. The difference between the temperature after thermal equilibrium has been reached and the initial temperature before heat is applied is used for determining the specific energy consumption $\Delta E/\Delta T$. It was found from 15 calibration measurements to be:

$$\Delta E/\Delta T = (11.67 \pm 0.10) \times 10^3 \text{ watt.sec}/^{\circ}C$$

4.2.2. Determination of the electron beam energy by means of the calorimeter

The calorimeter was set in the path of the electron beam, directly in front of the quantameter, and the beam was otherwise unimpeded. The power of the electron beam was chosen to be approximately equal to the heat power applied during calibration, i.e. between 100 and 200 W. The irradiation time necessary for a temperature rise of about $10^{\circ}C$ was between 10 and 20 min.

The lack of time prevented us from making more than three measurements with a beam energy of 2.9 Gev.

Figure 20 illustrates one of the measured temperature-time graphs. Unlike the case of the calibration graph, we have here a maximum which arises from the beam surrendering the major part of its energy in the first ten radiation lengths, so that the heat source is nearer the thermometer than during calibration. The temperature difference is determined in the same manner as during calibration. The results will be compared with the Faraday cage measurements in the following section.

4.3. Comparison of Faraday cage and calorimeter

Whilst the energy was measured with the calorimeter the total charge of the electron beam was measured with the secondary emission monitor. Before and after the calorimeter measurement, the secondary emission monitor was calibrated by means of the Faraday cage. The beam pulse and hence the beam energy were measured as described in Section 3.

The calibration constants and the beam data are listed in Table 1

for 2.9 Gev. Table 2 compares the total energy measured by the calorimeter and the total number of electrons, evaluated from the above by means of the beam energy, with the total quantity of electrons measured directly with the Faraday cage. Within the error limits of ± 0.7%, the two methods agree extraordinarily well, demonstrating the reliability of the charge measurement by means of the Faraday cage.

Table 1. Calibration constants of the calorimeter, the secondary emission monitor and the Faraday cage at 2.9 Gev.

Beam pulse or beam energy	(2.90 ± 0.015) Gev
Calibration constant of the calorimeter	$(11.67 \pm 0.10) \cdot 10^3$ watt.sec/°C = $(7.282 \pm 0.054) \cdot 10^{13}$ Gev/°C
Calibration constant of the calorimeter at 2.9 Gev	$(2.511 \pm 0.025) \cdot 10^{13}$ electrons/°C
Charge ratio Q_{FK}/Q_{SEM} at 2.9 Gev	1.954 ± 0.008
Measured relative charge loss of the Faraday cage at 2.9 Gev	$(1.9 \pm 0.9) \cdot 10^{-3}$
Corrected charge ratio Q_{FK}/Q_{SEM} at 2.9 Gev	1.956 ± 0.009
Calibration constant of the SEM at 2.9 Gev	$(1.221 \pm 0.006) \cdot 10^{19}$ electrons/a.sec

Table 2. Comparison of the calorimeter and the Faraday cage

Measurement no.	Charge of 10^5 [a.sec]	Temp. rise in calorimeter [°C]	No. of electrons measured with calorimeter ($\times 10^{-14}$)	No. of electrons measured with Faraday cage ($\times 10^{-14}$)	Diff. Faraday cage - calorimeter, %
1	2,185	10,63	2,669 ± 0,027	2,668 ± 0,012	- 0,04
2	2,161	10,46	2,627 ± 0,026	2,639 ± 0,012	+ 0,46
3	1,984	9,53	2,393 ± 0,024	2,423 ± 0,011	+ 1,25
				Mean	+ 0,56 ± 0,70

4.4. Gas-filled quantameter (GM)

4.4.1. Relative measurements

4.4.1.1. Dependence of the measured values on the beam position

The quantameter was moved by means of a trolley across the path of the γ-beam without any other changes in the beam geometry (beam 24). This gave the dependence of the measurement results on the beam position rela-

tive to the quantameter (Figure 21): the measured value is noticeably changed only when the well collimated γ-beam hits the inner edge of the radial correcting slots.

The usable working area of the quantameter has therefore a diameter of at least 18 cm.

4.4.1.2. Current-voltage characteristics (plateau measurements)

Before a gas-filled quantameter was used, it was first checked - by means of a plateau measurement - whether the gas discharge used for the measurement already exhibits, at the chosen beam intensity and spill-length*,

---

Translator's note: Term unfamiliar.

---

recombination effects due to the momentarily excessive ionization density.

Figure 22 shows three measured plateaus for 3 Gev, with the intensity of the external electron beam varying in the ratio of 1 - 10 - 100.

The plateaus measured for the intensities of about 10^6 and 10^7 electrons per pulse have similar inclinations of about 1.5-2% in the straight part. In the plateau measurement with 10^6 electrons per pulse,

the individual results are much more scattered because of a wrongly chosen integration constant. On the other hand, when the intensity is 10^8 electrons/pulse, the plateau rises by more than 5% and its absolute value is lower as well: the measurement is in this case obviously upset by the recombination.

Strictly speaking, the decisive factor for the recombination is not the number of electrons per pulse, but the ratio of this number and the spill-length which gives the number of generated ion pairs per unit time. This is valid for periods which are long as compared to the travel time of electrons or ions in the gas discharge area; this is the case when the period is greater than 1 μsec.

It follows from the results shown in Figure 22 that the DESY quantameter filled with 95% argon and 5% CO_2 may be used when no more than 5×10^5 electrons, or effective γ-quanta, per microsecond hit the instrument (i.e. when the spill-length is say 200 μsec - about 10^3 electrons or effective quanta). Figure 23 shows the usable working range.

Unfortunately, the spill-length could be determined only very inaccurately, and the numerical values must be regarded as approximate.

A further source of uncertainty is that there is no quantitative criterion of whether a plateau is usable. Indeed, the inclination of the measured plateaus remains in existence even when the measurement is carried out with a much lowered intensity. Figure 24 illustrates this in the case of a weak γ-beam.

The effect is perhaps attributable to gas multiplication at edges and sharp points, which cannot be wholly avoided in practice.

For this reason, the verdict on a measured plateau is rather arbitrary. It is taken that a plateau is usable when its inclination and absolute value no longer vary with the reduced intensity. This was the reason for measuring the absolute values of the quantameter constants at the relatively low intensity of 10^7 electrons/pulse.

Figure 25 shows the plateaus corresponding to each absolute measurement, with normalized ordinate values.

4.4.1.3. Comparison of various quantameter

At the end of May 1965 we compared three (out of the five available) DESY quantameters on the basis of γ-beam 22 (one apparatus of type D1, no. 1 and four instruments of type D3, no. 2-5).

In every case, the gas-filled quantameter no. 5 was used as the reference instrument, and the intermediate standard was a thin ionization chamber with air atmosphere. Without changing the geometry of the beam, the quantameters could be changed from one apparatus to another. The results of the comparison tests are shown in Table 3.

Table 3. Comparison of gas-filled quantameters. The standard instrument is quantameter no. 5, filled with 95% Ar and 5% CO_2

Quantameter no. (n)	Energy (Gev)	Measured charge ratio Q_n/Q_5	Pressure-temperature ratio p/T torr/°K	Charge ratio recalculated for p/T = 2.700, Q_n^x/Q_5^x	Error	Mean value independent of energy	Surface
1	2,72 1,47	0,739 0,741	2,722 2,722	0,741 0,743	±0,004 ±0,004	0,742	Copper
2	2,75	1,002	2,714	1,007	±0,004	1,007	Gold-plated
3	2,86 1,63	0,982 0,975	2,734 2,734	0,981 0,974	±0,002 ±0,012	0,978	↓
4							
5 standard instrument	./.	./.	2,732	1000 (by definition)	./.	1,000	

The third column gives the results of direct measurements of the charge ratio Q_n/Q_5, which is recalculated in column 5 for the "normal gas filling" of 2.700 torr/^oK (corresponding eq. at 293^oK to a gas pressure of 790 torr). The basis for this normalization is:

$$Q_n^x \text{ (normalized)} = Q_n \text{ (measured)} \times p/T \times 1/2.700$$

The results of column 5 represent the instrument constants, dependent only on the geometry and the properties of the measuring plate assembly, and independent of the gas filling. Quantameter no. 1 - the only representative of the type D1 with copper plates and no gold plating - produced a current which, after elimination of the energy effect, was 25.8% smaller than the current measured with the gold-plated quantameters D3 no. 2, 3, and 5.

Compared to the standard instrument no. 5, the other three quantameters of type D3 differ only by 2.6% at the most, which means that they are virtually independent or the energy and identical within the overall design tolerances (column 7).

The surface properties were not taken into account in the theory

of gas-filled quantameters[1], and only the bulk effects are considered in the analysis of the quantameter constants.

Contrary to this theory, there appears to be a clear surface effect which is not yet explained theoretically. Attempts should be made to find an explanation for the discovered effect, for instance by experiments with ionization chambers the surface of which is gold- or silver-plated.

The possibility of surface effects even in quantameters with copper surfaces is perhaps indicated by the calibrating measurements of quantameters carried out at CEA[10], where differences of up to 11.3% were detected between the measured constants and their values calculated on the basis of the theory[1].

4.4.2. Measurement of the absolute values of calibration constants of gas-filled quantameters

The absolute value of the quantameter parameters was determined at 1.53, 2.90 and 4.85 Gev by exchanging quantameter no. 5 for the Faraday cage as the calibration standard. A secondary emission monitor served as the inter-

radiable standard instrument.

The Faraday cage measures only the number of electrons, so that knowledge of the primary electron beam energy E is also required. E was measured as described in section 3.

When the measured charges are Q_i, the quantameter constant K_e is

$$K_e = \frac{E}{e} \cdot \frac{Q_{TK}}{Q_{SEM}} \cdot \frac{Q_{SEM}}{Q_{\nu M}} \quad [\text{Mev.coul}^{-1}]$$

where E is the energy of the external electron beam in Mev,

e is the elementary charge in coulombs, and

Q_i is the measured charge in coulombs.

The results are shown in Table 4 and Figure 26.

Table 4. Measurements on the gas-filled standard quantameter no. 5

Energy in Gev	Measured constant K_e (Mev/coul)	Error (%)	Mean K_e (Mev/coul)	p/T (torr/^oK)	Normalized constant K_e^x (Mev/coul)
1,53	$3,48 \cdot 10^{18}$	2,2			
2,90	3,45	1,2	$(3,49 \pm 0,05) \cdot 10^{18}$	2,728	$(3,53 \pm 0,05) \cdot 10^{18}$
4,85	3,54	1,5			

Within the error limits, the results do not depend on the energy.

Normalizing to a p/T value of 2.700 torr/^{o}K, as in the comparison measurements with quantameters, we obtained for quantameter no. 5 the normalized constant $K_e^x = (3.53 \pm 0.05) \cdot 10^{18}$ Mev/coul.

Calibration constants measured with an electron beam can also be applied to measurements with a γ-beam. The correcting slot at the end of the plate assembly allows for the escaping part of the energy. It operates quite accurately as long as the shower curve falls exponentially.

Numerous Monte-Carlo computations carried out at DESY[4] have shown that the fall of the shower curve at the end of the plate assembly was not exactly exponential, so that the correcting slot produces a slight error.

Figure 27 illustrates the shower curve for incident electrons and for monochromatic γ-quanta of 6 Gev. The cross-hatched areas between the shower curves and the exponential law indicate that the error of the slot in correcting the energy loss for both primary electrons and monochromatic γ-quanta is about 1%.

Since the radiation spectrum of the synchrotron due to the retarding particles contains γ-quanta of all energy values up to a maximum, the above determined error of 1% represents the upper limit for single-energy γ-quanta of 6 Gev.

The calibration constants K_e measured with an electron beam may therefore also be applied to measurements of γ-rays without any corrections, and will provide an accuracy of $\pm$ 1.2%.

Table 5 shows the quantameter constants K_e^x, K_e, and K_γ, regarded at present as valid and obtained by multiplying the values measured for the standard quantameter no. 5 by the normalized quantameter ratio c_n/c_5 (see Section 4.4.1.1).

Table 5.

Quantameter no. (n)	Beam	Normalized ratio (Q_n/Q_5)	Normalized calibration constant K_e^x (Mev/coul)	Values accepted on Aug.1,1965	
				p/T (torr/°K)	Calibration constant K_e, K_γ in Mev/coul
1	16 e-p	0,742	$(4,75\pm0,09)\cdot10^{18}$	2,722	$(4,71\pm0,09)\cdot10^{18}$
2	24	1,007	(3,51±0,06)	2,714	(3,49±0,06)
3	22	0,978	(3,61±0,08)	2,734	(3,57±0,08)
4					
5	Standard instrument	1,000	(3,53±0,05)	2,728	(3,49±0,05)

4.4.3. Measurement errors

In relative measurements as in Section 4.4.1 only random errors have to be considered because the operation is always in the same range of the integrator with the SEM used as the intermediate standard. Generally speaking, only the top and bottom limits of the measured value are given in the results of Section 4.4.1, because in most cases only two individual measurements were carried out.

There were always five individual measurement results when it came to determining the absolute calibration constant values; their dispersion is shown in Figure 28. It is impossible to detect any systematic dependence on the time factor.

The influence of partial errors on the total error is shown in Table 6.

Table 6. Errors in the measured calibration constants of the gas-filled quantameters

				Error	
Energy (Gev)	Measured constant (Mev/coul.)	Random measurement error (%)	Energy calibration (%)	Connect.* FK - SEM (%)	Random mean error (%)
1,53	$3,48 \cdot 10^{18}$	±0,55	± 2,0	± 0,8	± 2,2
2,90	3,45	±0,69	± 0,5	± 0,8	± 1,2
4,85	3,54	±0,70	± 1,0	± 0,8	± 1,5

Translator's note: Abbreviation uncertain; it could stand for "connections" or "estimate".

4.5. Secondary emission quantameter

4.5.1. Relative measurements

4.5.1.1. Influence of the beam position on the measurements

Because of a fault in our trolley, the change of quantameter position relative to the beam could be simulated only by shifting the electron beam by means of the last deflection magnet (Figure 5, 0807 M), while the quantameter remained always in the same position.

Figure 29 shows how unsatisfactory was the result of these measurements: the relative sensitivity curve changes in the central region by about 5%.

Figure 9 shows a Polaroid photograph of the electron beam of 4.24 Gev used in the measurements: in addition to the required heavily overexposed beam core, there are on both sides additional parts which were not blanked out by a collimator. When the beam is shifted laterally with respect to the quantameter, these parts of the beam hit in a varying manner the walls of the beam duct tube between the magnet and the quantameter.

Varying scatter of these parts of the beam may change the measured values by as much as 5%, because of the grazing incidence in the correcting slots of the SE_2.

This interpretation is still to be checked by measurements with a well collimated γ or electron beam, with the quantameter shifted across the beam, but it is supported by the fact that no such error was detected with other secondary-emission quantameters[6].

4 . 5 . 1 . 2 . Current - voltage characteristics

The current-voltage characteristics of the secondary emission quantameter, which correspond to the plateau of a gas-filled quantameter, are illustrated in Figure 30 for the electron beams of 1.78, 2.20 and 4.24 Gev.

When $|U| < 30$ v, the measured values change greatly with the applied voltage; there is a maximum at $|U| = 30$ v and the drop at $|U| = 500$ v amounts to 5%. The graph plotted for $E = 1.78$ Gev was presumably measured wrongly at voltages above 30 v because of an undetected fault, which is also indicated by the much greater scatter of the measured points. It follows from these measurements that nearly all measured secondary electrons are emitted in the low-energy spectrum, $\varepsilon < 30$ ev; the same was found

for thin secondary emission monitors (SEM) (see Figure 12 and ref. 7).

The current of the secondary-emission quantameter hardly changes with the voltage in the area of the maximum intensity ($|U| \approx 30$ v) in contrast to the gas-filled quantameter which has no similar area. In this area, the secondary-emission quantameter is therefore a standard independent of the measurement parameter.

The values measured at 2.90 Gev are once more plotted in Figure 31, together with the values obtained using the γ-beam of 2.82 Gev. (The ordinates are made comparable by normalization.) The measured graphs agree perfectly when $|U| < 200$ v, and differ only by at the most 2.5% when $|U| \geq 200$ v.

4.5.2. Absolute value of the calibration constant of the secondary emission quantameter

The absolute value of the calibration constant was found for the secondary-emission quantameter using the external electron beam of 1.78, 2.90 and 4.24 Gev and the Faraday cage as a standard instrument (see equation in

Section 4.4.2); the secondary-emission monitor was applied as the intermediate standard.

The center of gravity of the beam was in these measurements in the axis of the plate assembly in the quantameter ("zero position" in Figure 29). We have already drawn attention to the lack of reliability in the measurements of the beam position effect (Section 4.5.1.1); this is allowed for in the present case by an additional error of ± 2.5%.

Lack of time made it impossible to repeat the measurements with the quantameter changing position and with a better collimated beam.

Table 7 and Figure 32 bring the results of the measurement of the calibration constant.

Table 7. Calibration constants of the secondary-emission quantameter no. 5

Energy (Gev)	Measured constant, K_{es} (Mev/coul)	Error (%)
1,78	$1{,}360 \cdot 10^{21}$	± 3,7
2,90	1,339	± 3,5
4,24	1,317	± 3,5

The measured calibration constant in the investigated energy range is independent of energy within the error limits of ± 3.5%.

Contrary to the QM, the correcting slot contributes to the measured current only with a weight of one slot, and a rise in the calibration constant might be expected in the investigated energy range as the primary energy of the beam is increased, because the quantameter used as a secondary-emission meter is too short and the measured current should therefore be too small. It is impossible to say that this is not the case, within the limits of error.

The calibration constant measured with an electron beam can also be applied in the case of bremsstrahlung radiation. We have already pointed out, in Section 4.4.2 and Figure 25, that the absorption of energy by a quantameter without a correcting slot is not the same for electron radiation and for monochromatic γ-radiation. At 6 Gev the energy loss of primary monochromatic γ-radiation is 3.4% greater than that of primary electrons. This difference ought to be smaller in the case of bremsstrahlung radiation which contains quanta of all energy levels up to the maximum.

The results of the Monte-Carlo computations are not yet available, and it is not possible to integrate over the bremsstrahlung radiation spectrum. Nevertheless, the calibration constant measured with an electron beam may also be used for γ-rays, within the error limits of $\pm$ 3.5%. The error which then occurs is certainly less than 1%.

It would be interesting to calibrate the ΔE_2 with a calorimeter on a γ-beam. However, this is not yet possible because the intensity of γ-rays in DESY is only about one hundredth of that of the external electron beam and is too small for accurate measurements with the DESY calorimeter.

It was shown in Section 4.5.1.2 and Figure 31 that the current-voltage characteristics of an electron beam of 2.90 Gev and of a γ-beam of 2.82 Gev have virtually identical relative courses. This indicates that the measured value is strongly independent of the character of the shower, i.e. of whether the latter is produced by a primary electron or a γ-beam.

Figure 33 shows how the calibration constant is related to the intensity: over four powers of ten the calibration constant is independent of the electron beam intensity.

The greatest and decisive advantage of the secondary-emission quantameter as compared to the gas-filled quantameter is its linearity.

4.5.3. Measurement errors

Scatter of individual measurement results is substantially smaller for both relative (4.5.1) and absolute measurements (4.5.2) than in the case of the gas-filled quantameter; the mean dispersion error is in the SEQ only a few parts per thousand whereas it is about 2% in the gas-filled quantameter.

This seems to indicate once more, in an indirect manner, that the SE_Q is independent of the intensity. Dispersion of measurements with the gas-filled quantameter, carried out with the same intermediate standard, is much greater; the explanation may be that in spite of the applied low intensities saturation and recombination effects occur when the instantaneous beam flux is very high, and such effects may cause the greater dispersion of results.

Errors of absolute measurements are shown in Table 8.

Table 8. Errors in determining the calibration constant of the secondary-emission quantameter

Energy (Gev)	Measured constant K_{es} (Mev/coul.)	Measurement errors					
		Random error (%)	Energy calibration (%)	Connect.* FK/SEM (%)	Random mean (%)	Uncertainty of beam position error (%)	Total error (%)
1,78	$1,360 \cdot 10^{21}$	± 0,12	± 1,0	± 0,8	± 1,24	± 2,5	± 3,7
2,90	1,339	± 0,09	± 0,5	± 0,8	± 0,95	± 2,5	± 3,5
4,24	1,317	± 0,14	± 0,5	± 0,8	± 1,04	± 2,5	± 3,5

Translator's note: Abbreviation uncertain; it could stand for "connections" or "estimate".

There is no evidence in Figure 34 that the results depend on time. The random error is small as compared with the errors of the energy calibration and of the ratio Q_{FK}/Q_{SEM}. However, all the other errors add up to only one half of the error of ± 2.5% introduced by the uncertainty in the beam positioning.

If the measurements were repeated with a sharply collimated beam, the error could probably be reduced to less than ± 1.3%.

4.6. Comparison of the two types of quantameters

The gas-filled DESY quantameter may be used with intensities of up to 5×10^5 electrons, or equivalent numbers of quanta, per μsec (4.4.1.2). If the spill length is say 200 μsec, this corresponds to approximately 1×10^8 particles per machine pulse.

Since the effective spill length cannot be accurately determined because of the fluctuations, the above conclusion must be regarded only as an indication of the correct order of magnitude.

The above intensity limit is just about reached in the γ-beams used in DESY, and it is just possible to apply the gas-filled quantameter with the standard atmosphere of 95% Ar and 5% CO_2.

At CEA the working range of the gas-filled quantameter is extended by a factor of six by using an atmosphere of 90% He and 10% N_2.

However, it is much simpler and more reliable to apply the quantameter only in the form of secondary-emission apparatus. The 33% is independent of intensity in the entire intensity range available in DESY

(4.5.2). This also permits us to avoid all errors due to the variation in the spill length.

Moreover, the calibration constant is a function only of the geometry and the surfaces in the apparatus, and does not depend on pressure or the composition and purity of the atmosphere. Dimensional errors which can occur during manufacture of the parts and assembly of the plates do not affect the results.

Vacuum control in the SE_γ is always possible through the mains supply of the ion getter pump outside the quantameter area, and operational faults (leaks) are detected at once.

All this supports the secondary-emission quantameters as the only apparatus to be used in future for all γ-beams operating at full intensity.

On the other hand, gas-filled quantameters can possibly be more convenient for γ-rays of lower intensity, because they produce greater currents (by a factor of 390) than the SE_γ. Thus, even at low intensities of the γ-beam, use can be made of the high accuracy of the DESY integrator ($\pm$ 0.5%), whereas the SE_γ would produce a current insufficient for the integrator.

There are still two limitations regarding the use of secondary-emission quantameters which must be removed by further measurements; these are:

1. Long-term stability of the secondary-emission quantameter has not been studied as yet.
2. When the SEQ was used, measurements of the deflected beam produced results which are far from clear (4.5.1.1) because the beam was not well collimated. However, this uncertainty will certainly be removed when the measurements are repeated with a well collimated beam.

We are grateful to the Synchrotron Operating Group (S1 and S2) for their help in the measurements. Only the very stable operation of the external electron beam and of the synchrotron made it possible to carry out a major part of the experiments.

The ejected electron beam was made available for our measurement by F22; W. Schmidt built the beam duct.

Group S2 developed the method used in the energy determination

without which the calibration experiments would be impossible.

F. Peters helped us greatly and unselfishly in constructing the measuring setup and in the measurements themselves.

All workers in A2 contributed to the measurements by their help in bulding the equipment and we are very grateful to them and to all other groups at DESY who gave us their support.

oooooooooooo

References

1. R.R. Wilson, Nuclear Instr. 1 (1957) 101-106. A more detailed description is given by A.P. Komar et al. in Sov. Phys.-Techn. Phys. 5, 11 (1961) 1299-1309.
2. K.L. Brown and G.W. Tautfest, Rev. Sci. Instr. 27 (1956) 696.
3. H. Nagel, Inst. of Physics, Bonn University, Electron-photon cascades in lead and Monte-Carlo calculations for primary electron energies between 100 and 1000 Mev.
4. U. Völkel, Electron-photon cascades in lead for primary particles with an energy of 6 Gev, DESY Report 65/6 (1965) and private communication regarding copper.
5. e.g., B. Rossi, High Energy Particles, p. 264 (1956).
6. H. Fischer and C. Schaerf, Stanford HEPL 309 (1963).
7. D.B. Isabelle and P.H. Roy, Nucl. Instr. and Meth. 20 (1963) 17-20.
8. S.A. Blankenburg, J.K. Cobb, and J.J. Muray, Stanford SLAC - PUB - 78 (1955).
9. G.W. Tautfest and H.R, Fechter, Rev. Sci. Instr. 26 (1955) 229.
10. J. de Pagter and M. Fotino, Cambridge, CEAL - 1022 and R. Fessel and J.R. Rees, Cambridge, CEAL - TM - 141.
11. F.A. Bumiller and E.B. Dally, Proc. Internat. Conference of Instrumentation in High Energy Physics, Berkeley, Calif. (1960) p. 305.
12. V.J. Vanhuyse and R.E. van de Vijver, Nucl. Instr. Meth., 15 (1962) 65.

Index of Tables

Index of Figures

Figure 1. Section through the Faraday cage

Abb. 1: Faraday-Käfig
schematisch

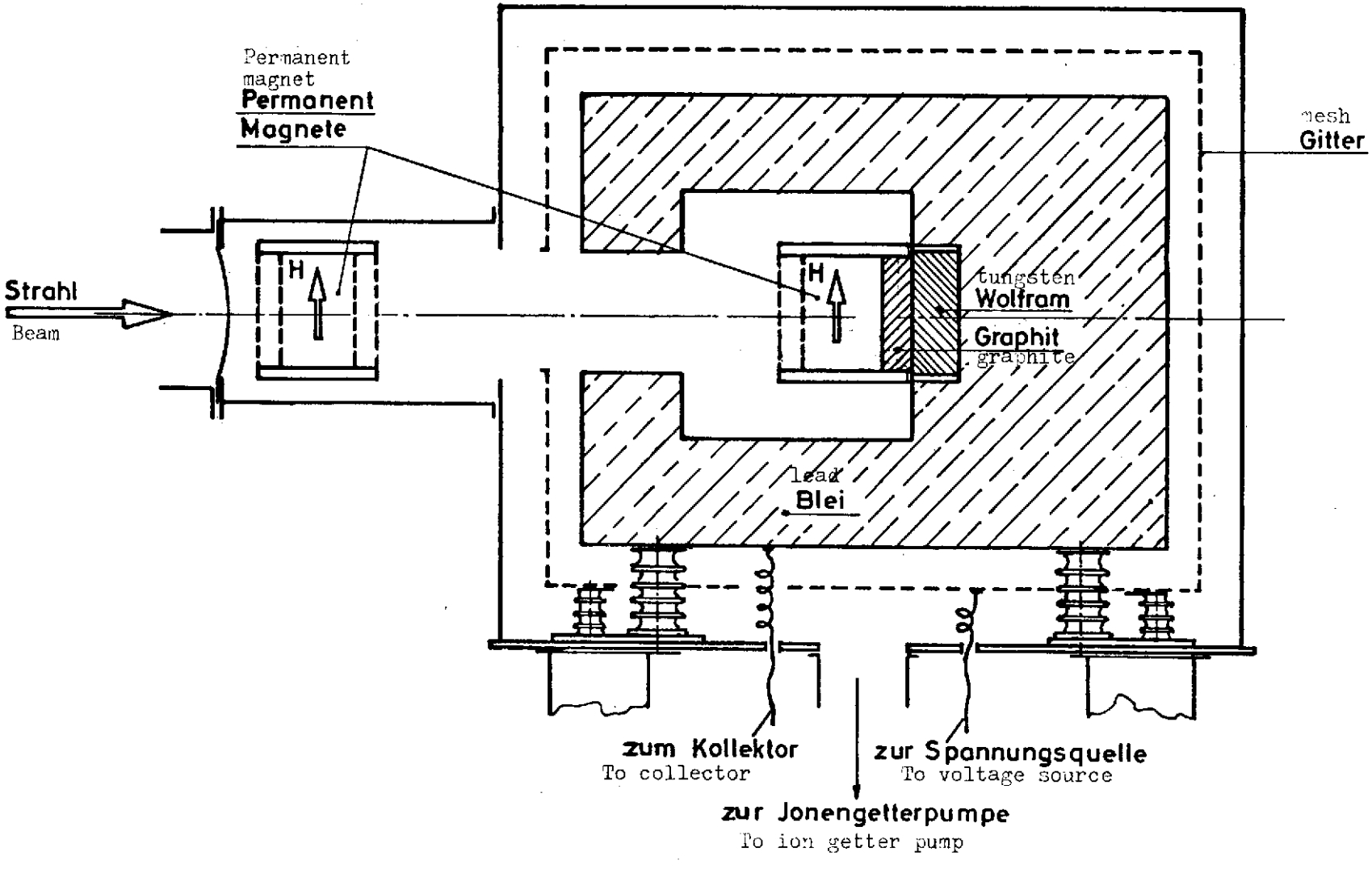

Figure 2. Section through the secondary-emission monitor

Abb. 2: Sekundäremissionsmonitor

schematisch

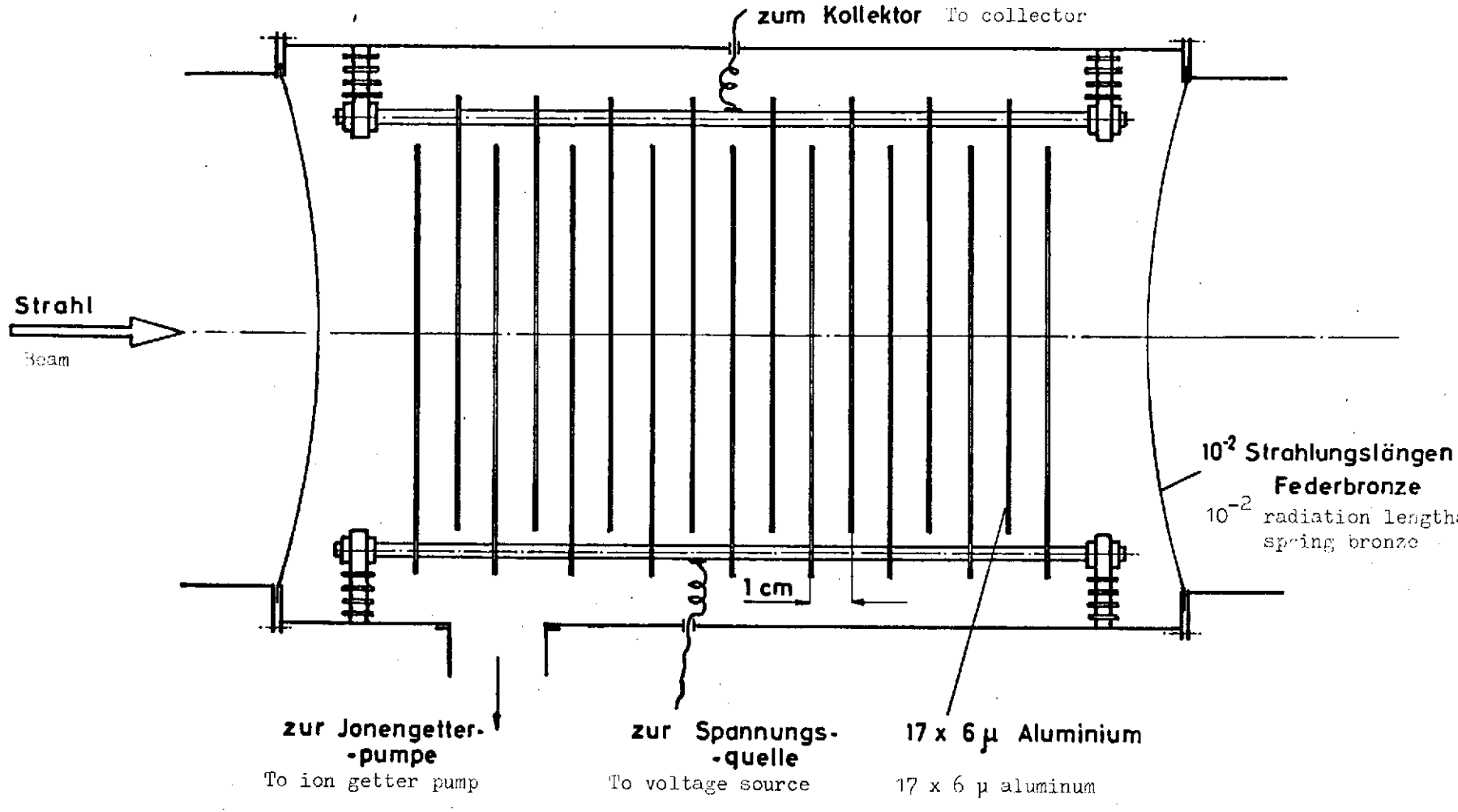

Figure 3. Section through the calorimeter

Abb. 3: Kalorimeter (schematisch)

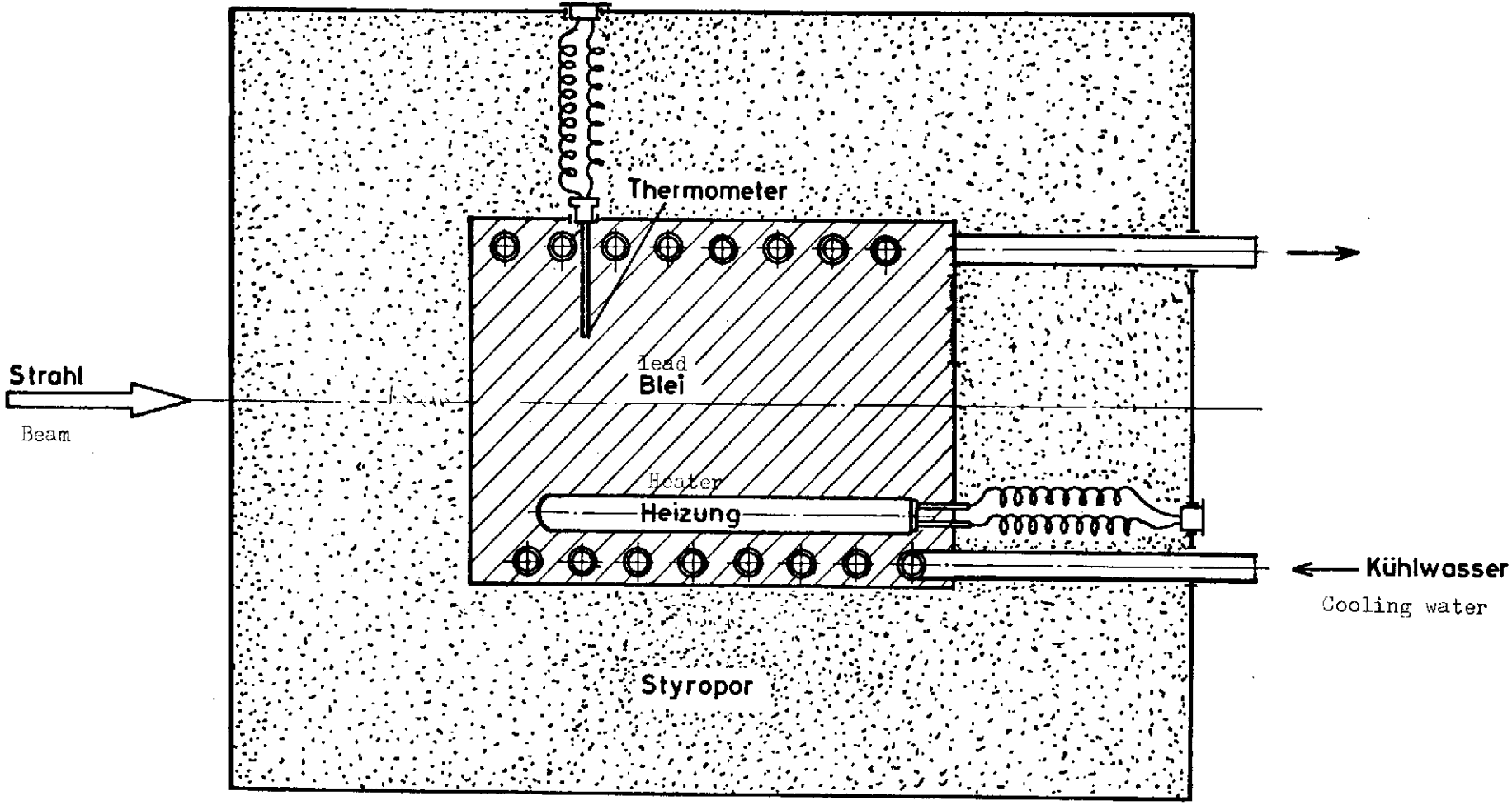

Figure 4.

Abb. 4:
Messpaket des Quantameters (schematisch).

Measuring plate assembly of the quantameter

A. R.R. Wilson's quantameter

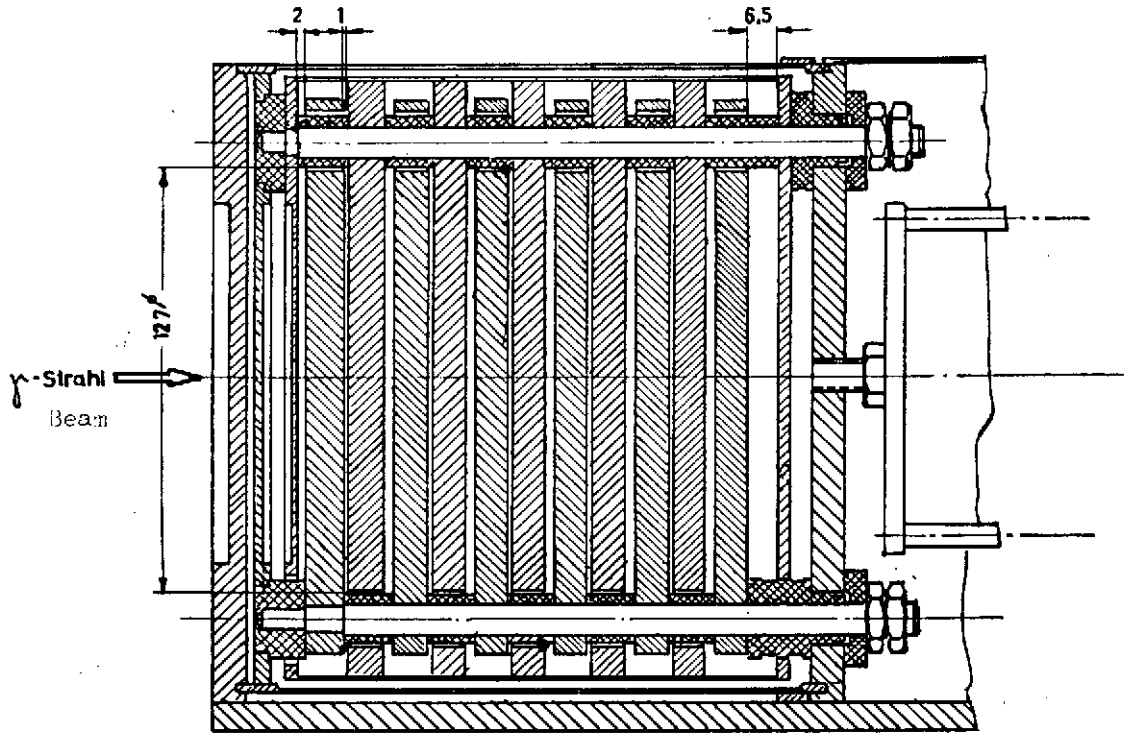

B. DESY-Quantameter

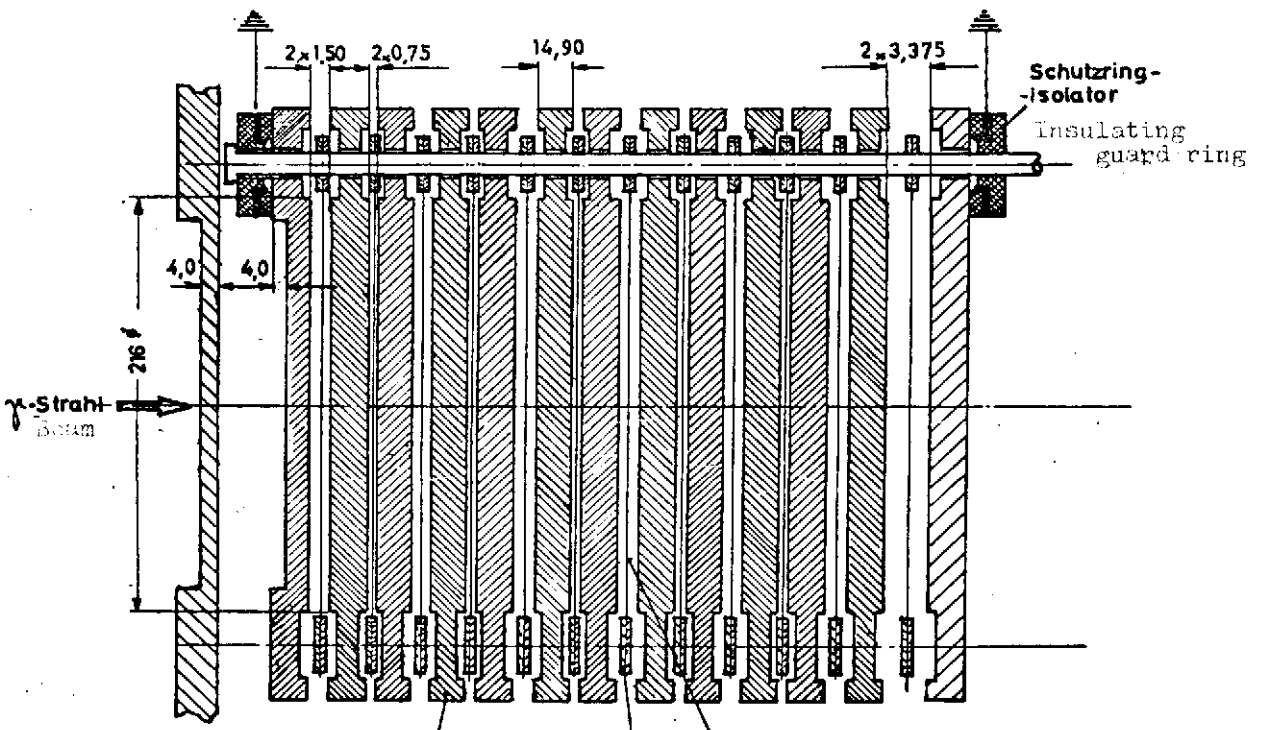

Figure 5.

Abb. 5.

Strahlaufbau für die Eichmessungen

Beam travel in calibration measurements

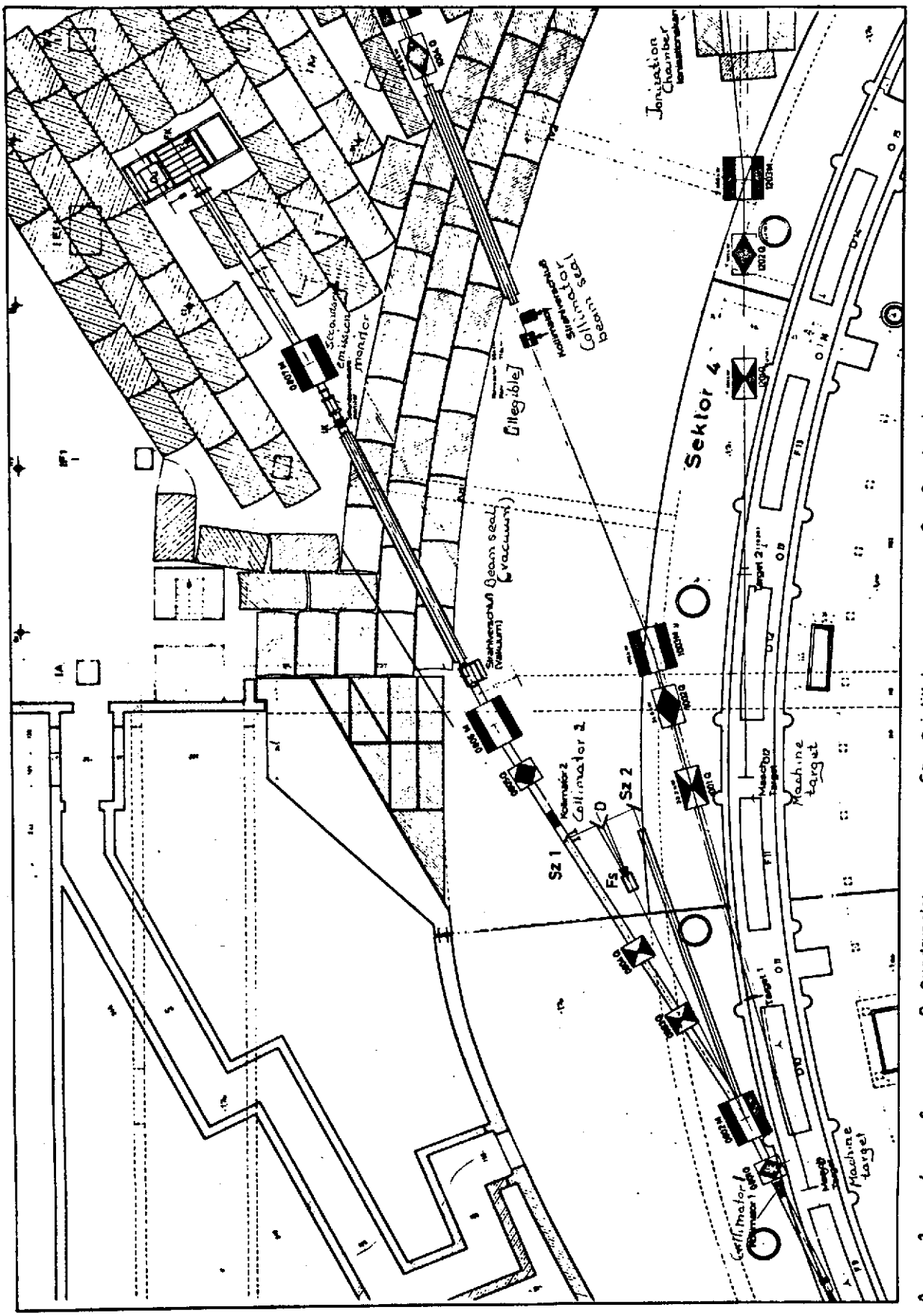

Figure 6

Arrangement of the secondary-emission monitor and ionization chamber in front of the third deflecting magnet

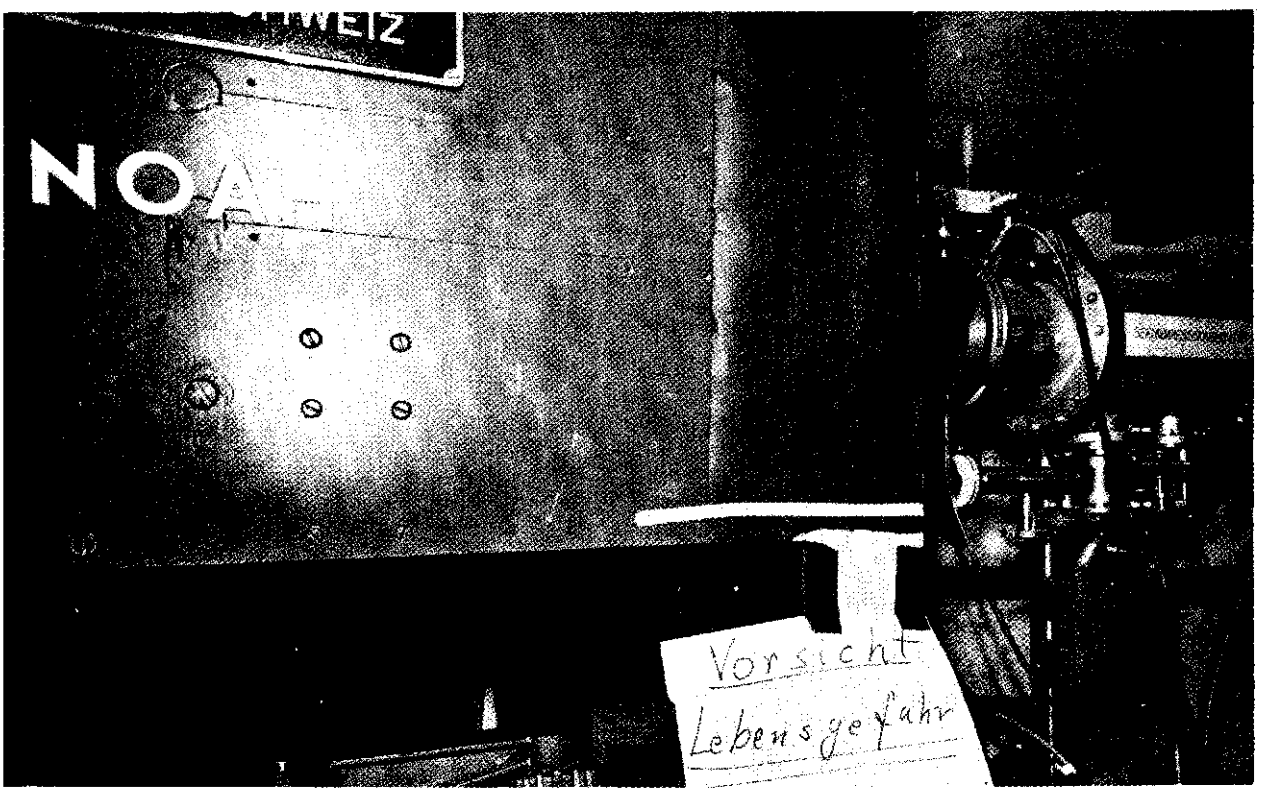

Figure 7

Quantameter and Faraday cage mounted on the trolley. The Faraday cage is in the path of the beam.

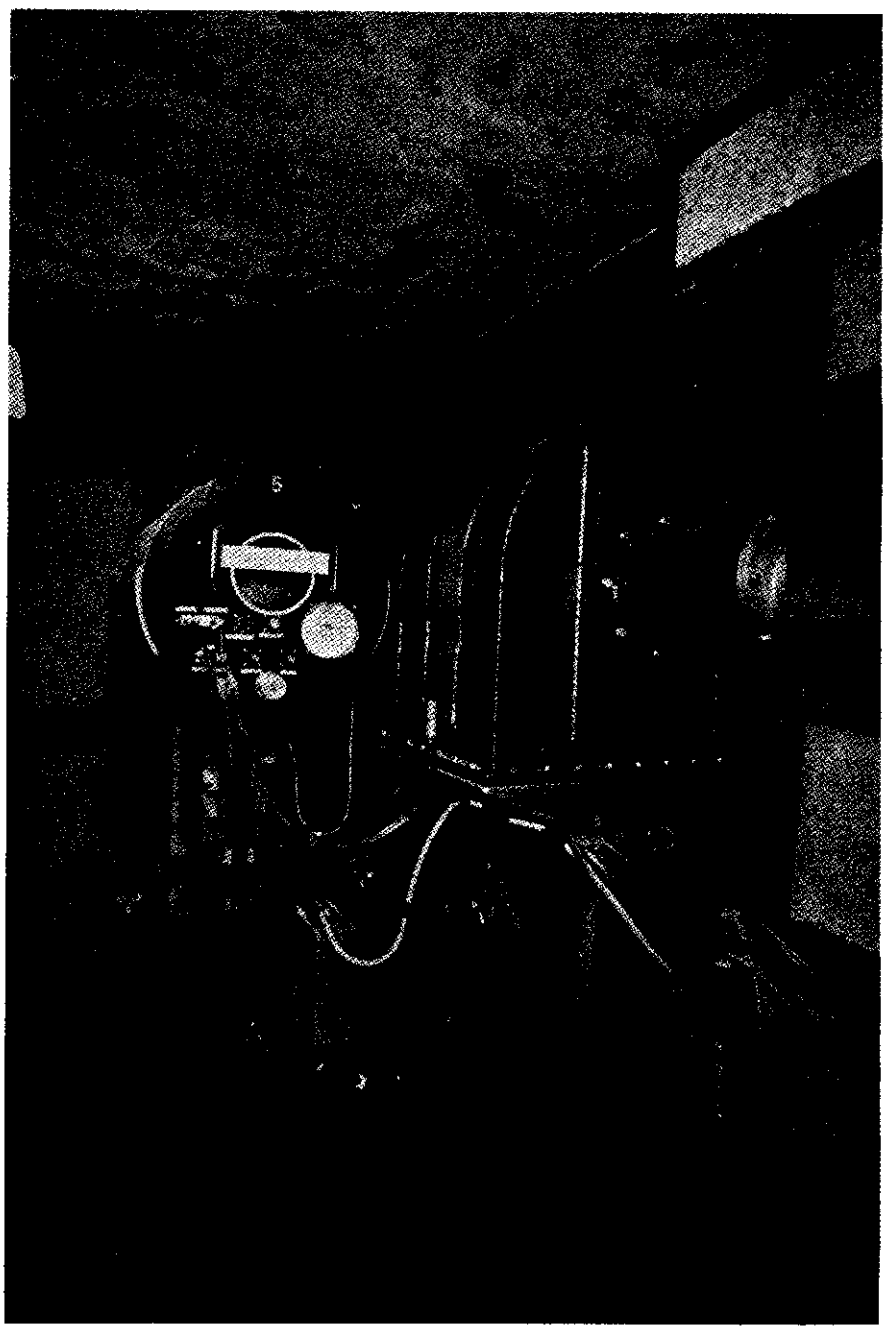

Figure 8

Electron beam of 3.0 Gev in front of the Faraday cage (looking along the beam direction)

Figure 9

Electron beam of 4.24 Gev in front of the Faraday cage. - Part of electrons with insufficient energy can be seen to the left of the greatly over-exposed beam core; to the right - a residue of scatter particles.

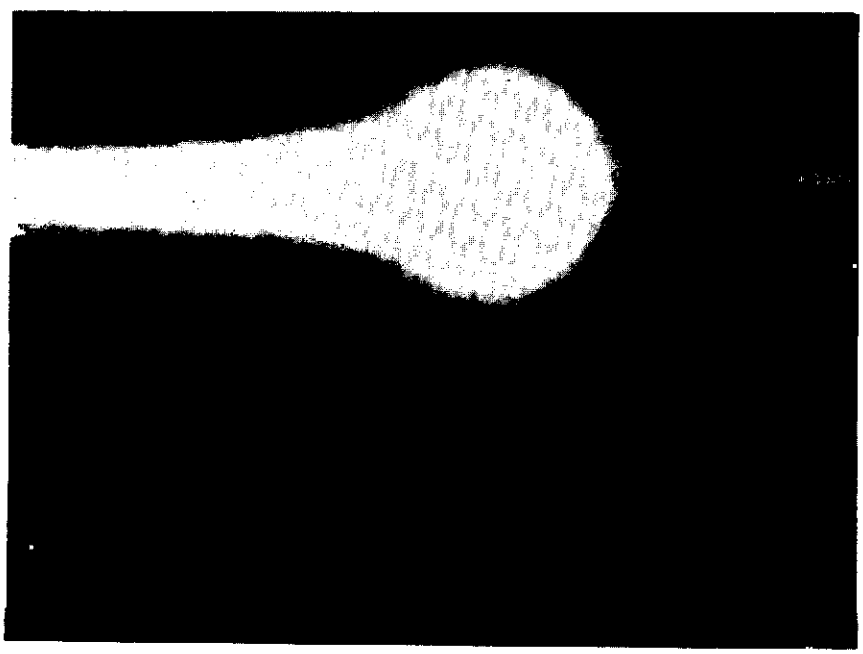

Figure 10. Short-term stability of the SEM

Abb. 10: Kurzzeit - Konstanz des SEM

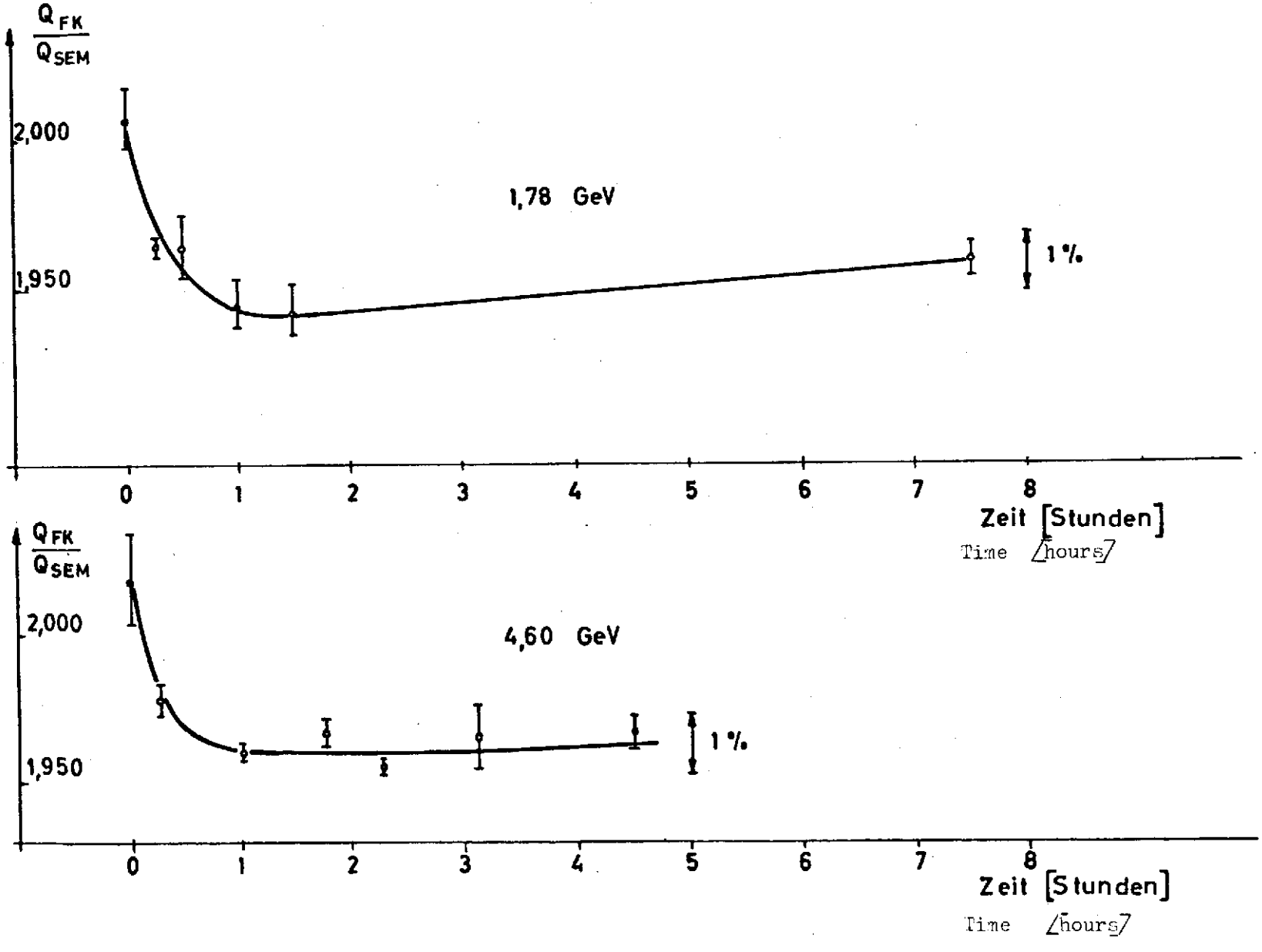

Figure 11. Long-term stability of the SEM

Abb. 11: Langzeit-Konstanz des SEM

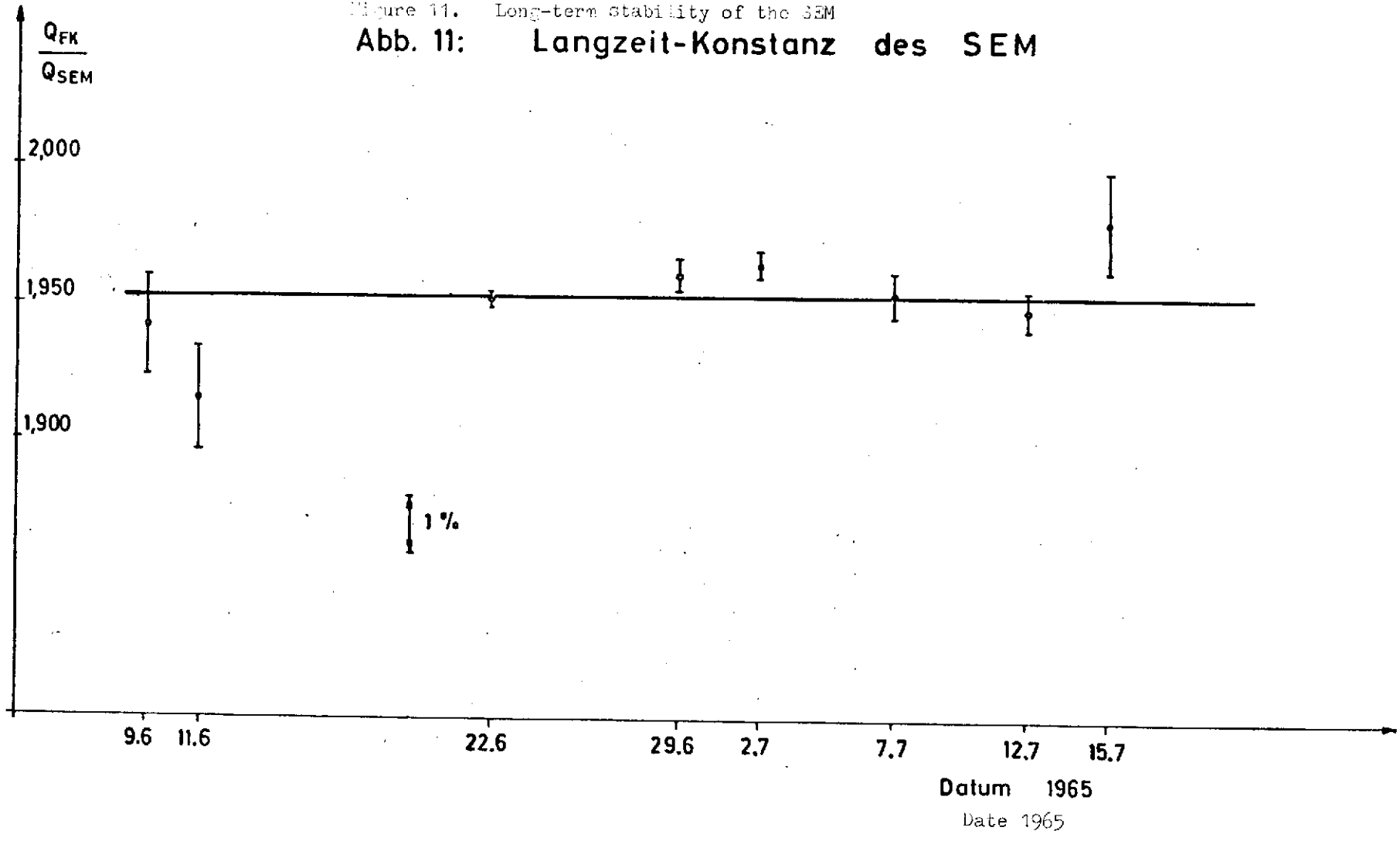

Figure 12. Plateau of the SEM at 2.9 Gev

Abb. 12: Plateau des SEM bei 2,9 GeV

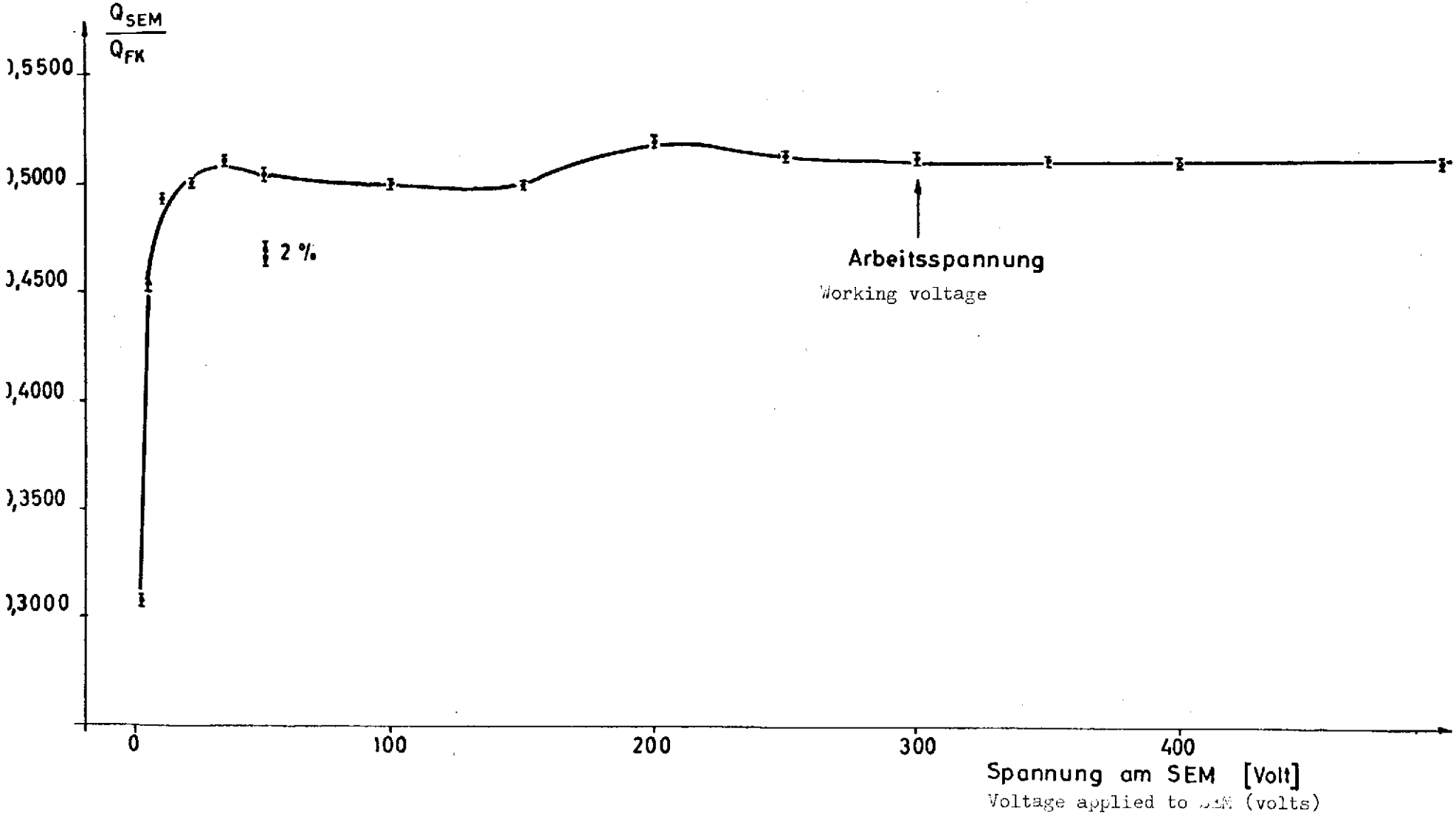

Figure 13. Dependence of the SEM on the intensity

Abb. 13: Intensitätsabhängigkeit des SEM

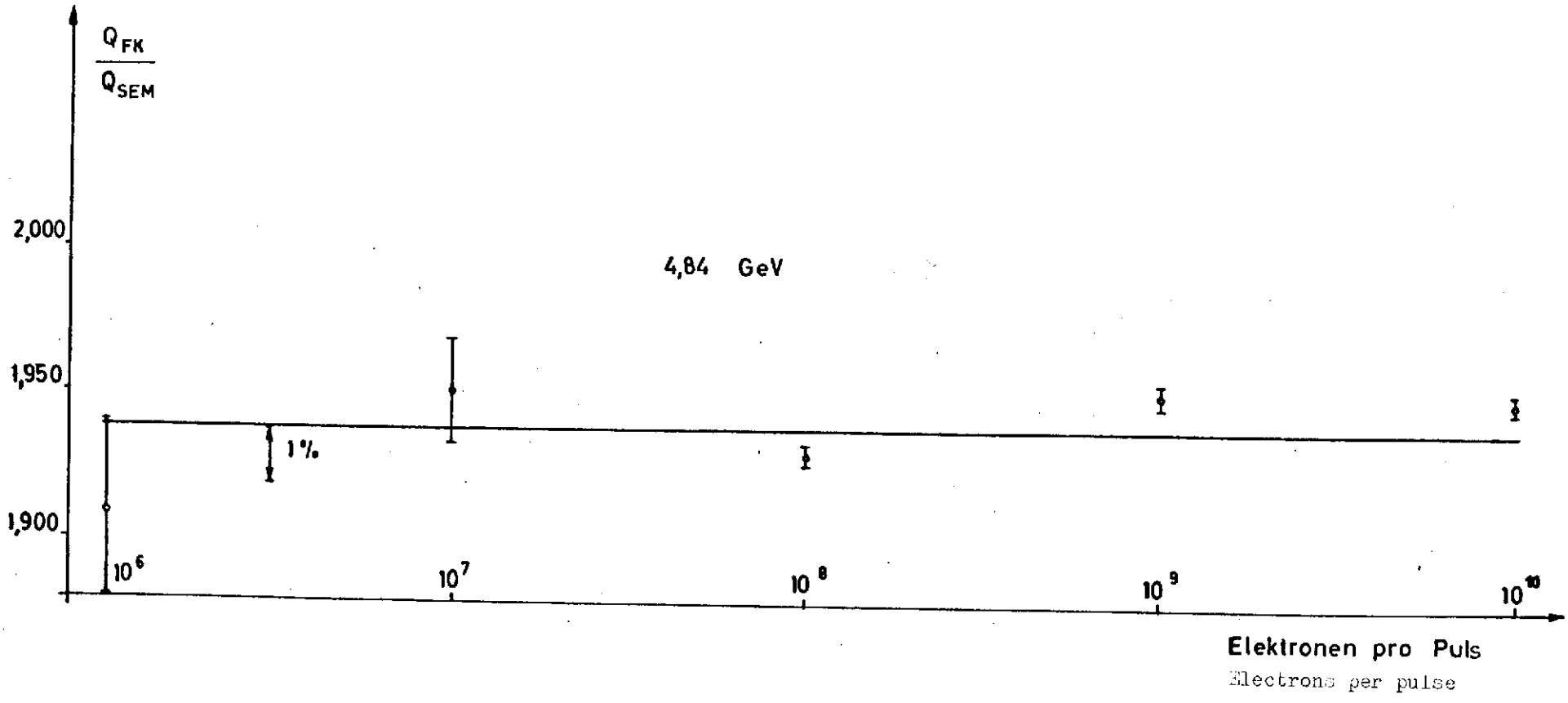

Figure 14. Dependence of the SEM on the energy

Abb. 14: Energieabhängigkeit des SEM

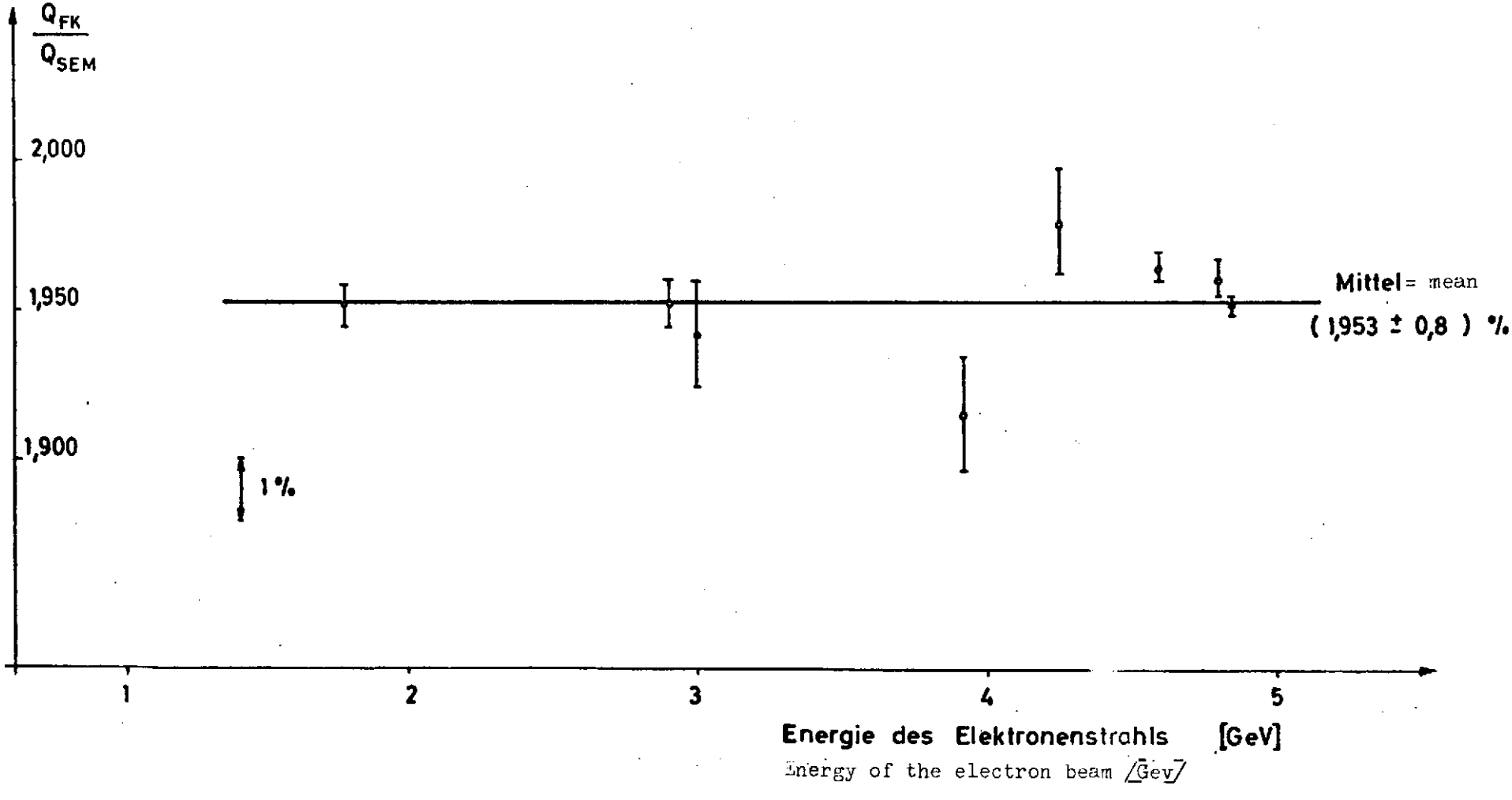

Figure 15. Charge loss in the Faraday cage at 2.9 GeV

Abb. 15: Ladungsverlust des Faraday-Käfigs bei 2,9 GeV

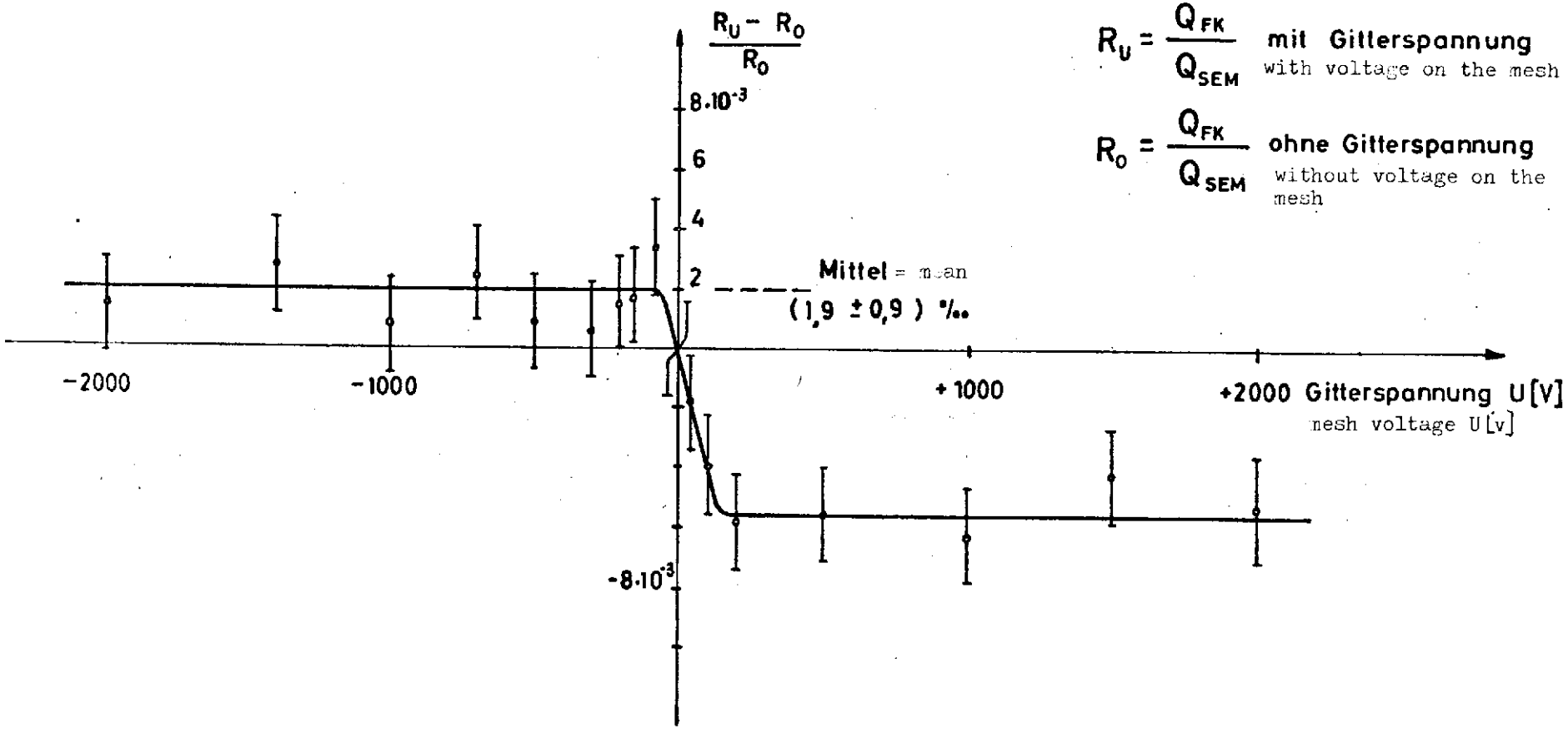

Figure 16. Charge loss in the Faraday cage at 4.6 Gev

Abb. 16: Ladungsverlust des Faraday-Käfigs bei 4,6 GeV

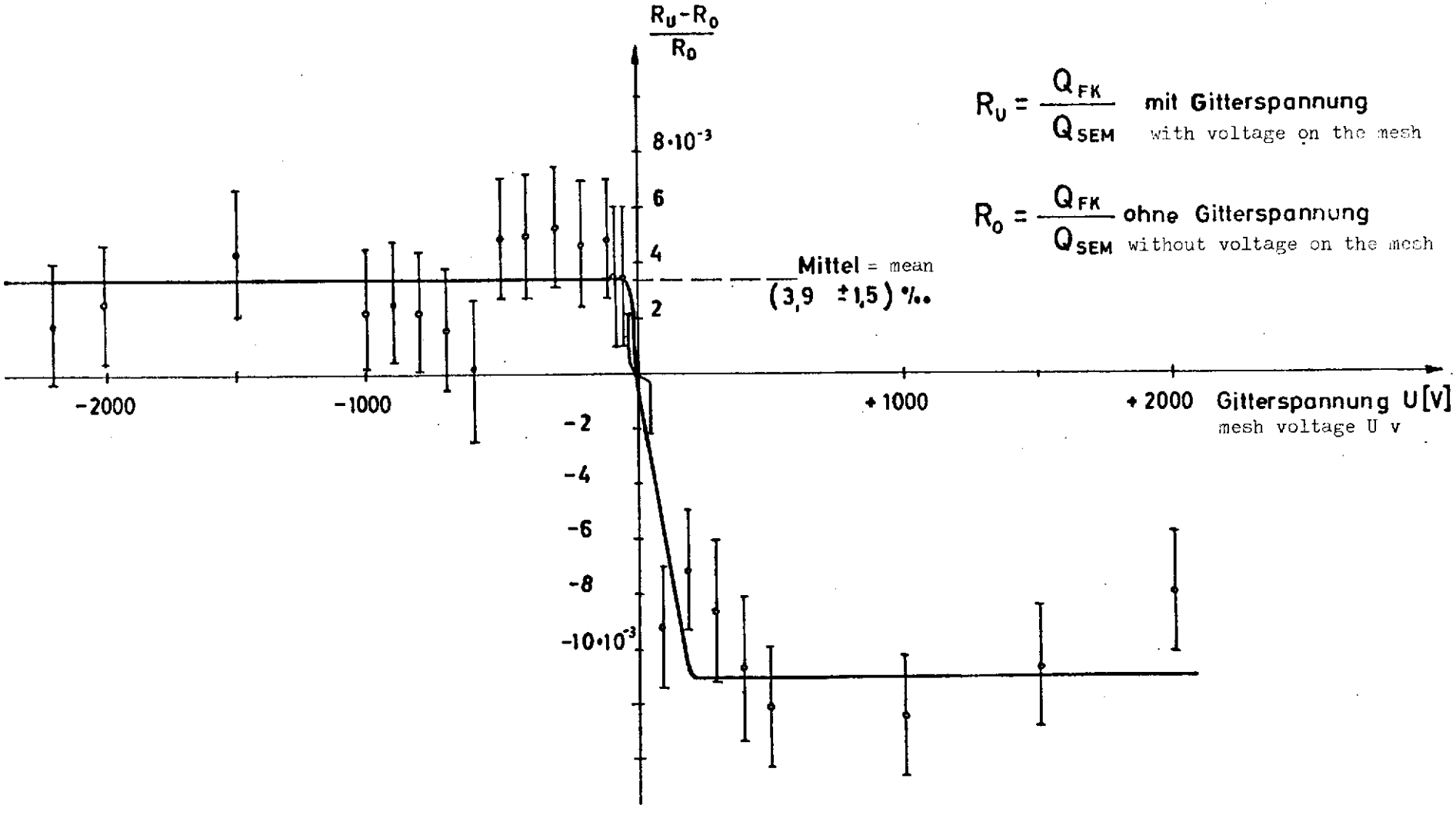

Figure 17. De_endence of the Faraday-cage on the energy

Abb. 17: Energieabhängigkeit des Faraday-Käfigs

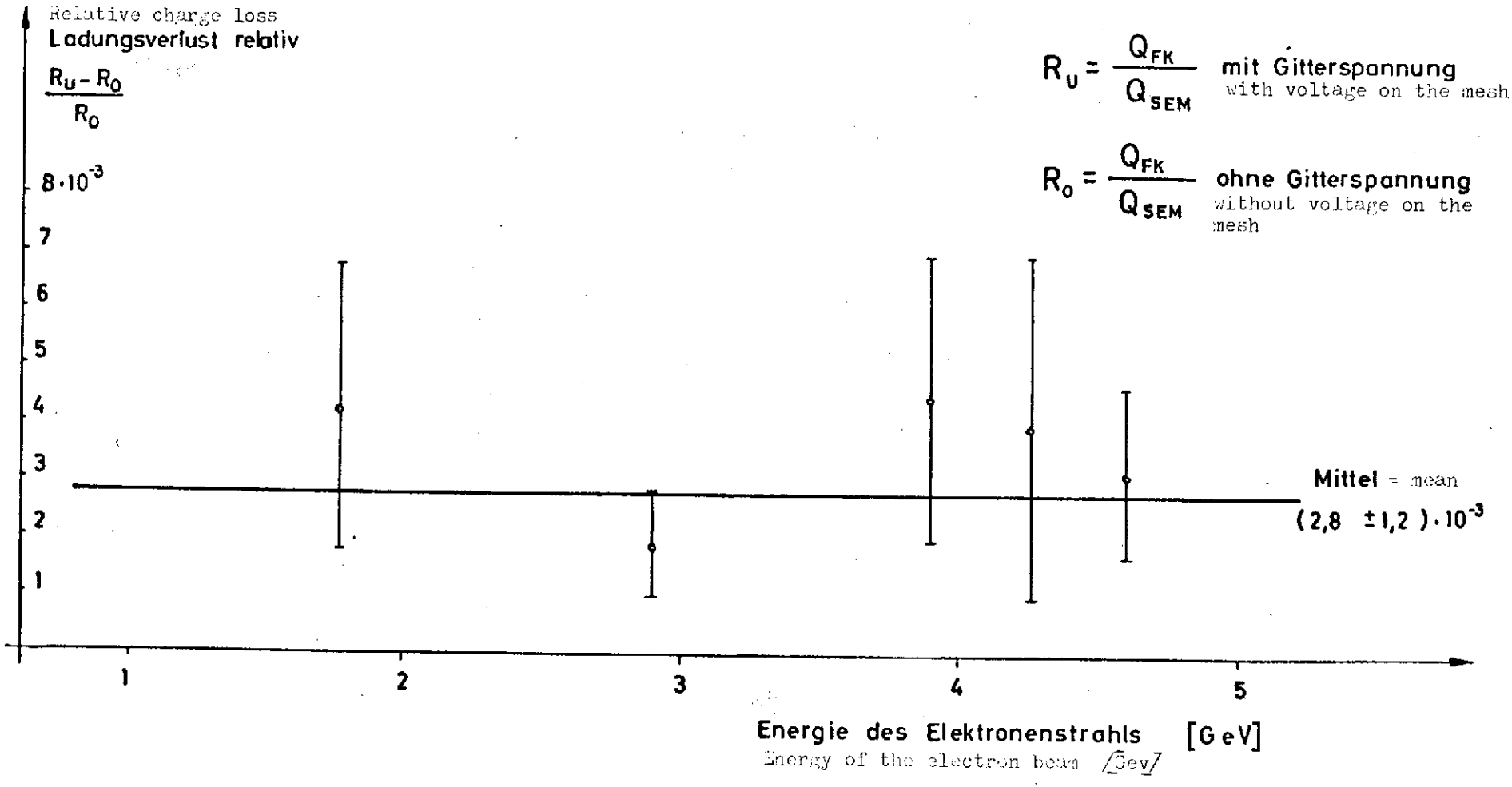

Figure 18. Useful aperture of the Faraday cage

Abb. 18: Nutzbare Öffnung des Faraday-Käfigs

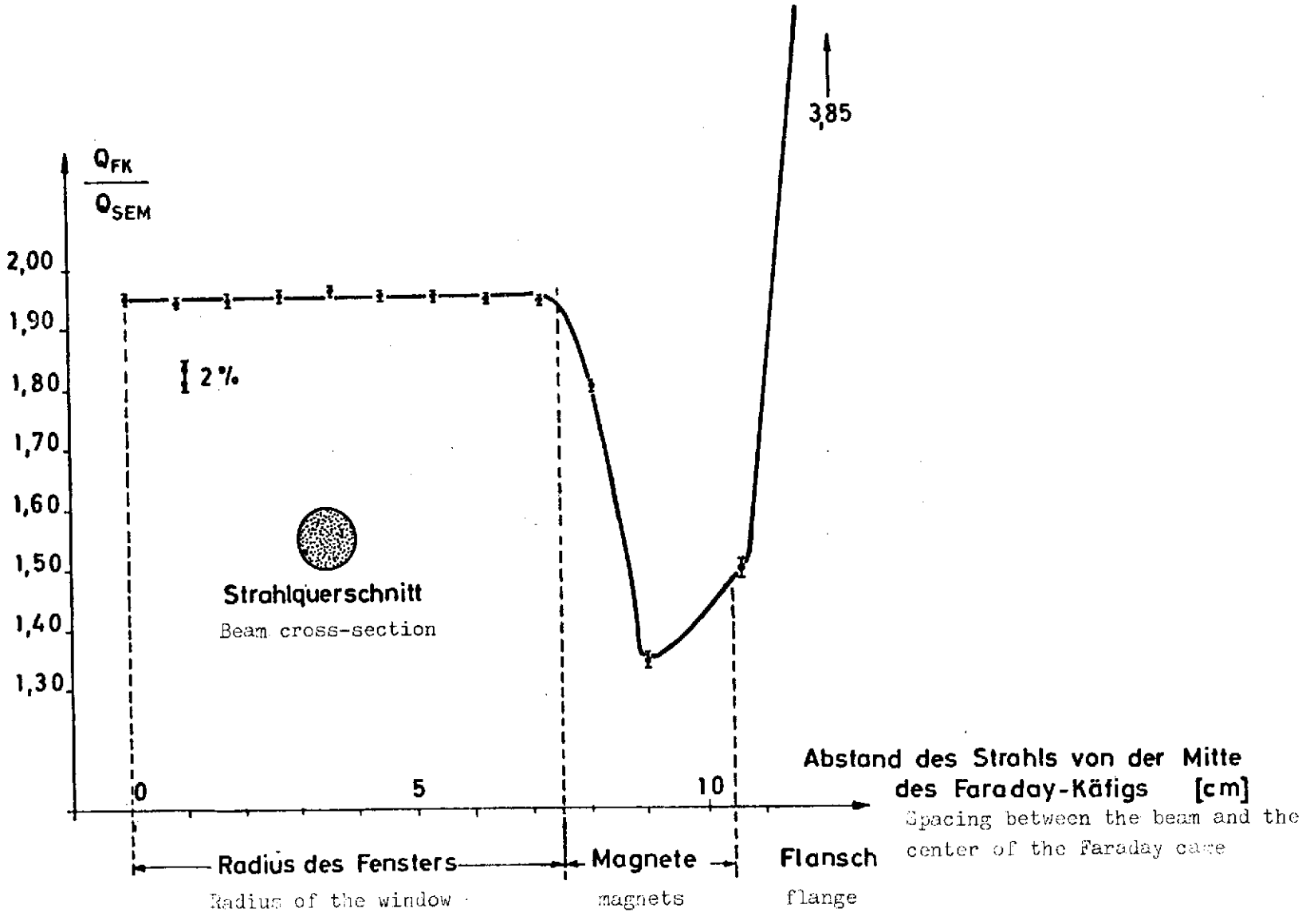

Fig. 19. Temperature/time plot of the calorimeter during calibration

Abb. 19: Temperatur-Zeit-Kurve des Kalorimeters bei der Eichung

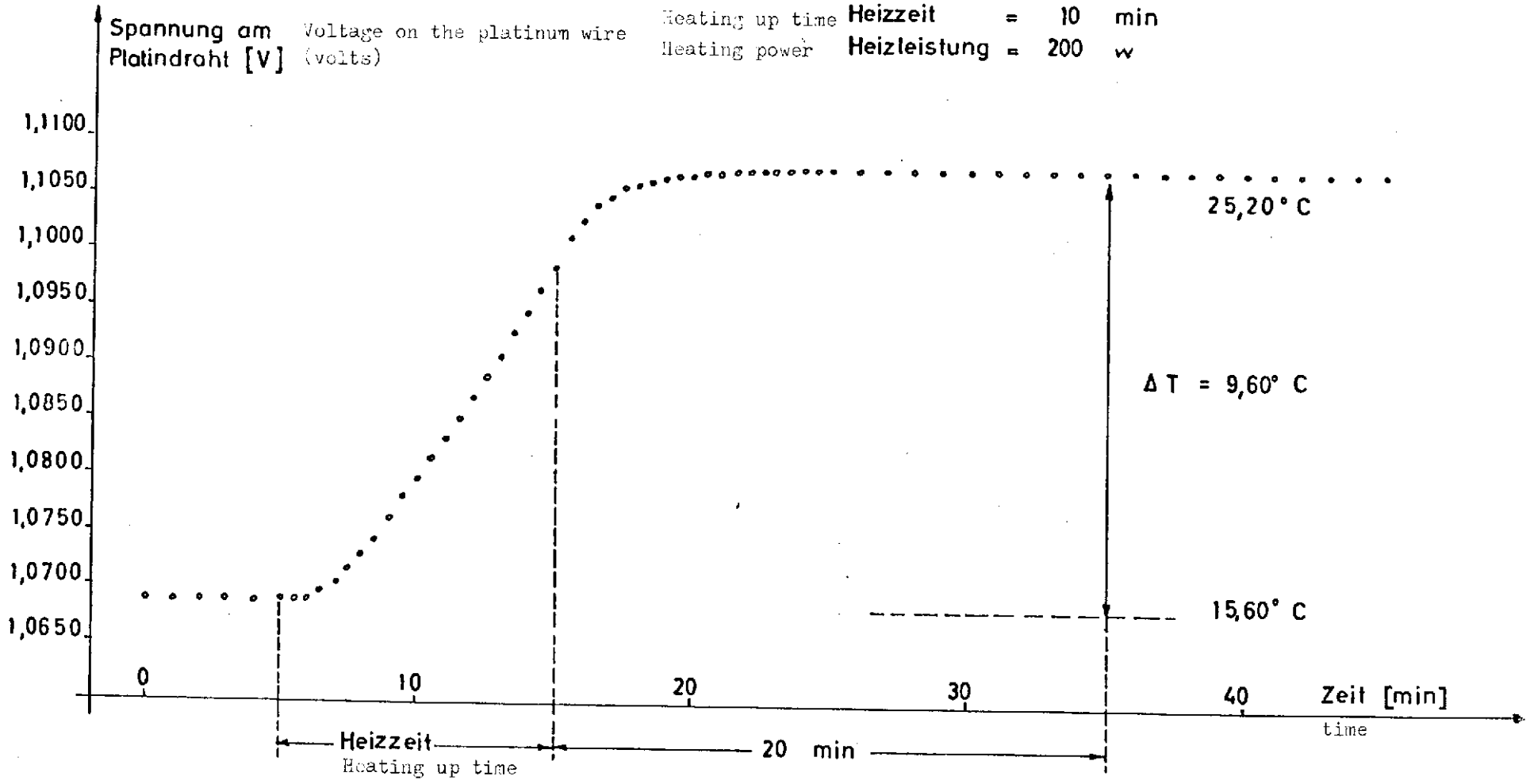

Figure 20. Temperature/time plot of the calorimeter during irradiation with 2.9 Gev

Abb. 20: Temperatur-Zeit-Kurve des Kalorimeters während einer Bestrahlung bei 2,9 GeV

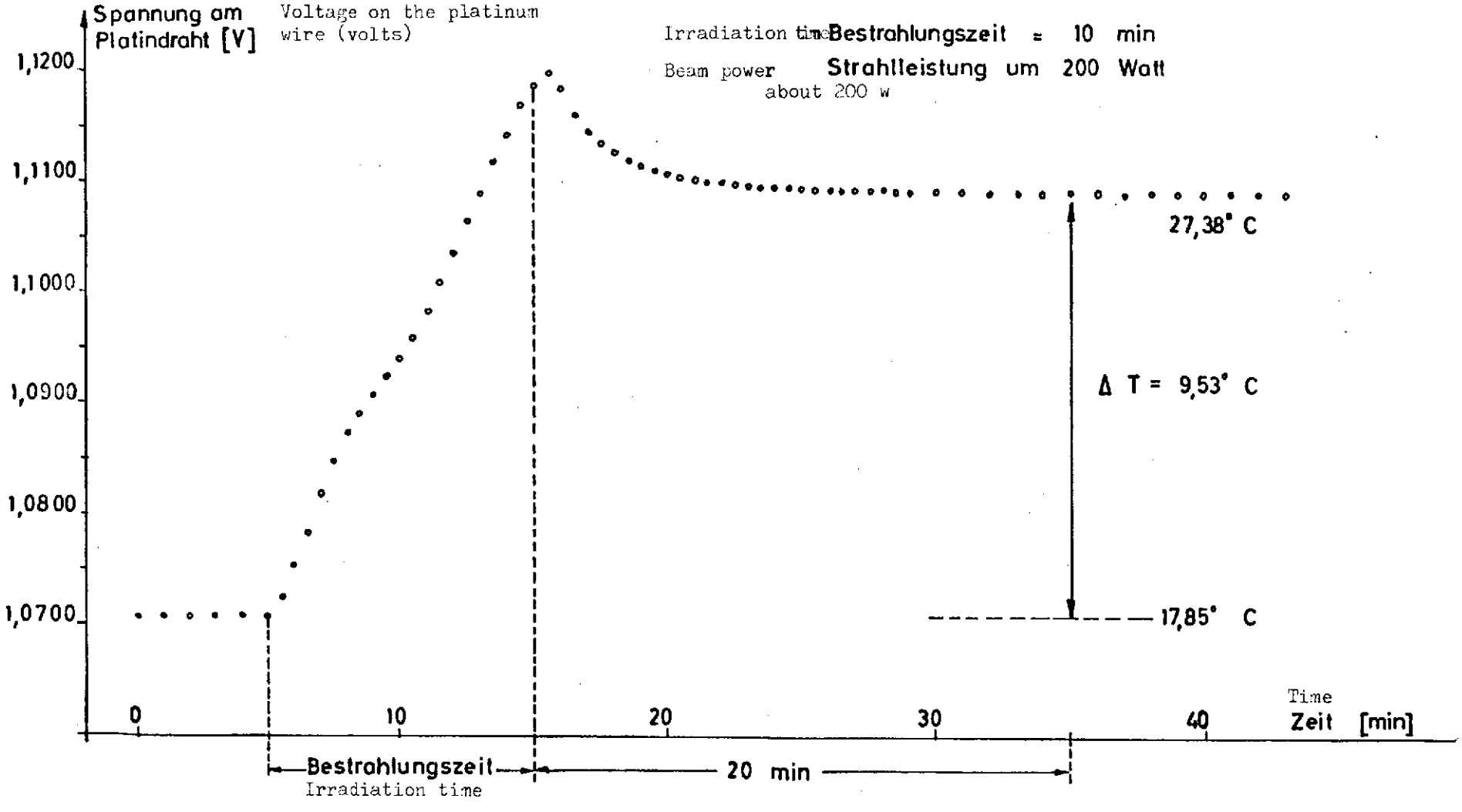

Figure 21

Lateral shifting of the gas-filled quantameter no. 5 in the path of the beam

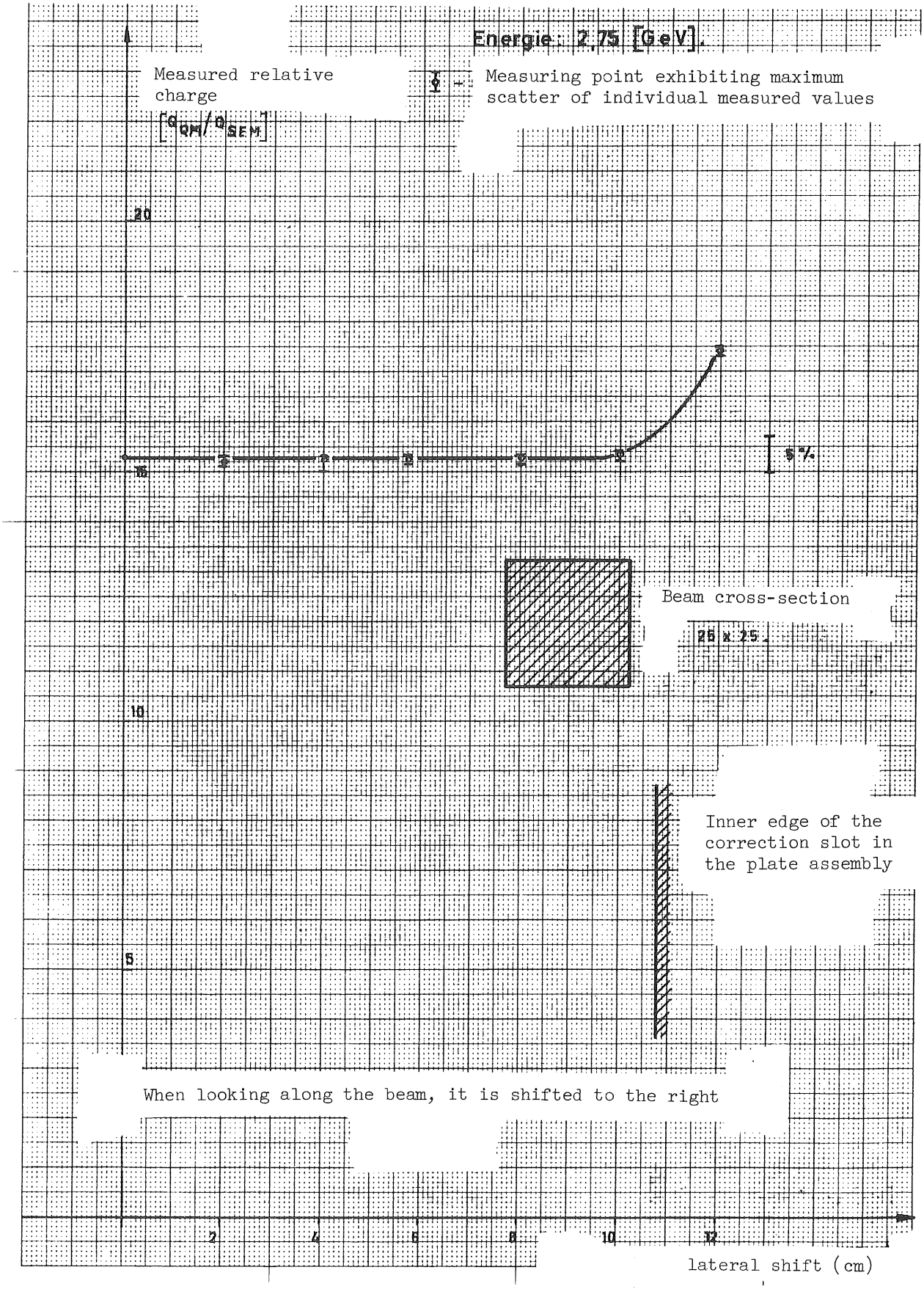

Figure 22

Plateau of the gas-filled quantameter no. 5 at 3.0 Gev as a function of the intensity

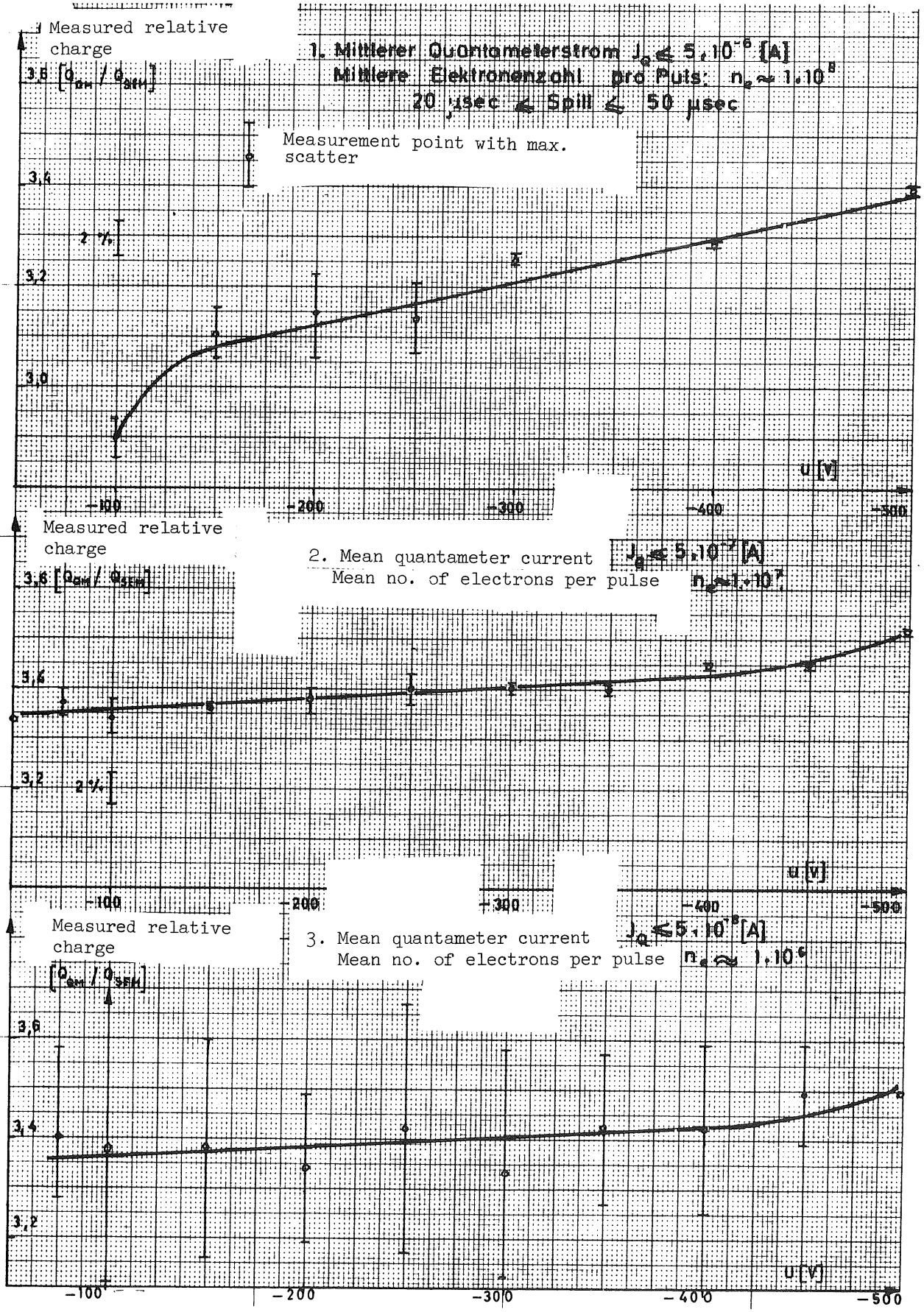

Figure 23

Relation between the spill length and the permissible number of particles per pulse in the gas-filled quantameter

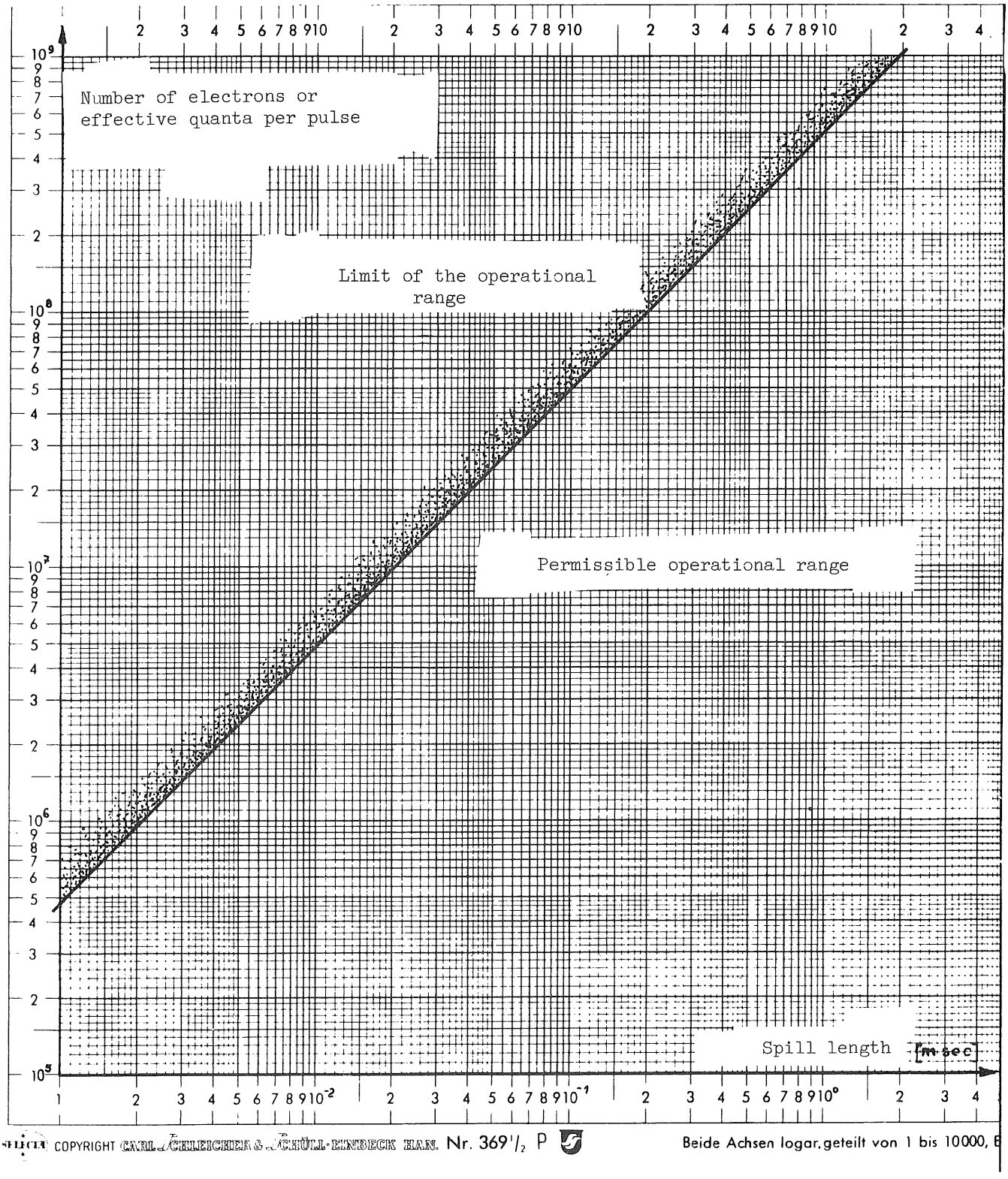

Figure 24

Plateau of the gas-filled quantameter no. 2 at 2,8 Gev. primary γ-beam of small intensity

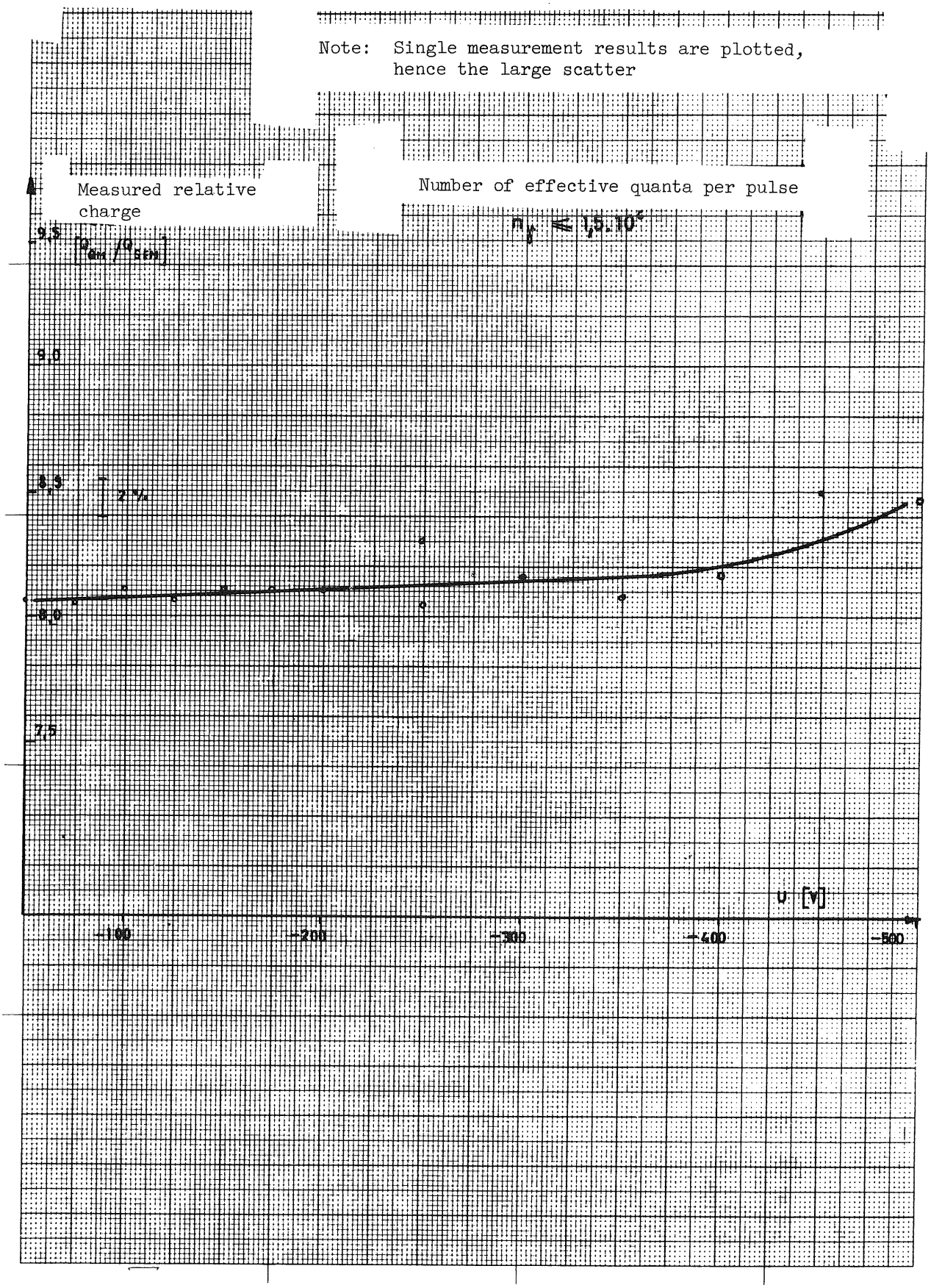

Figure 25

Plateau of the gas-filled quantameter no. 5 while the quantameter constants were determined

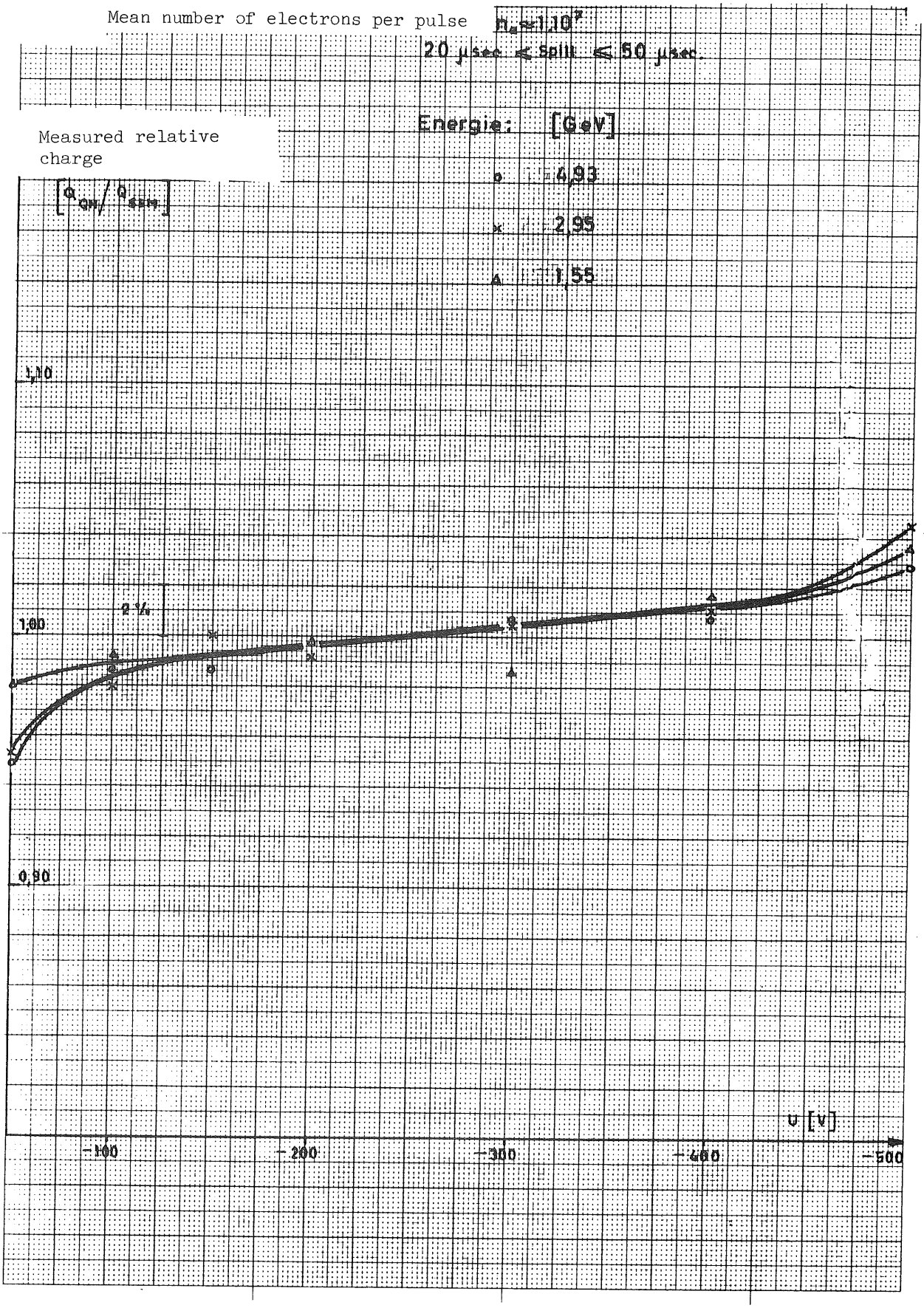

Figure 26

Measured calibration constant of the gas-filled quantameter no. 5 as a function of the energy

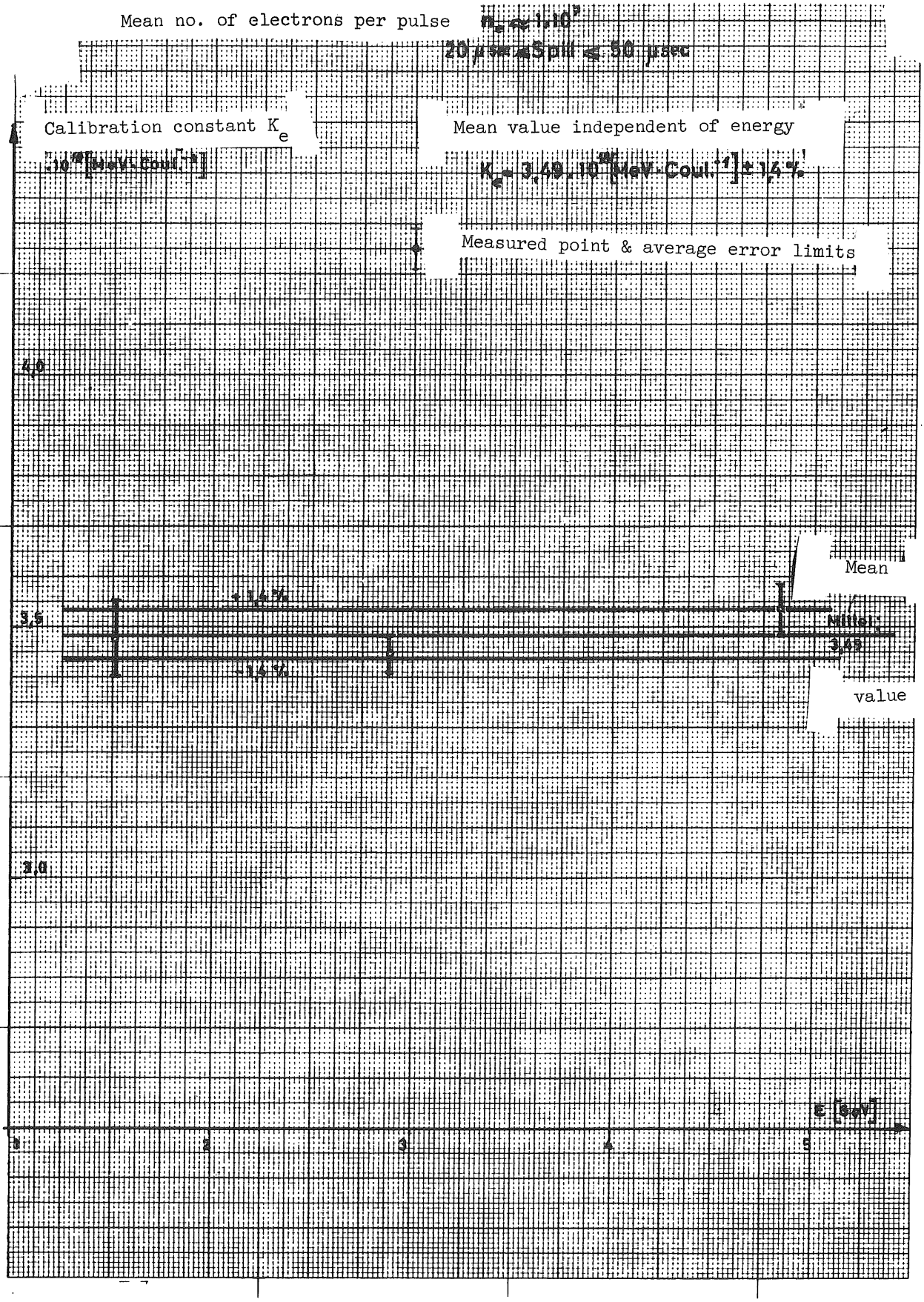

Figure 27

Energy distribution of the shower in DESY quantameter at 6 Gev

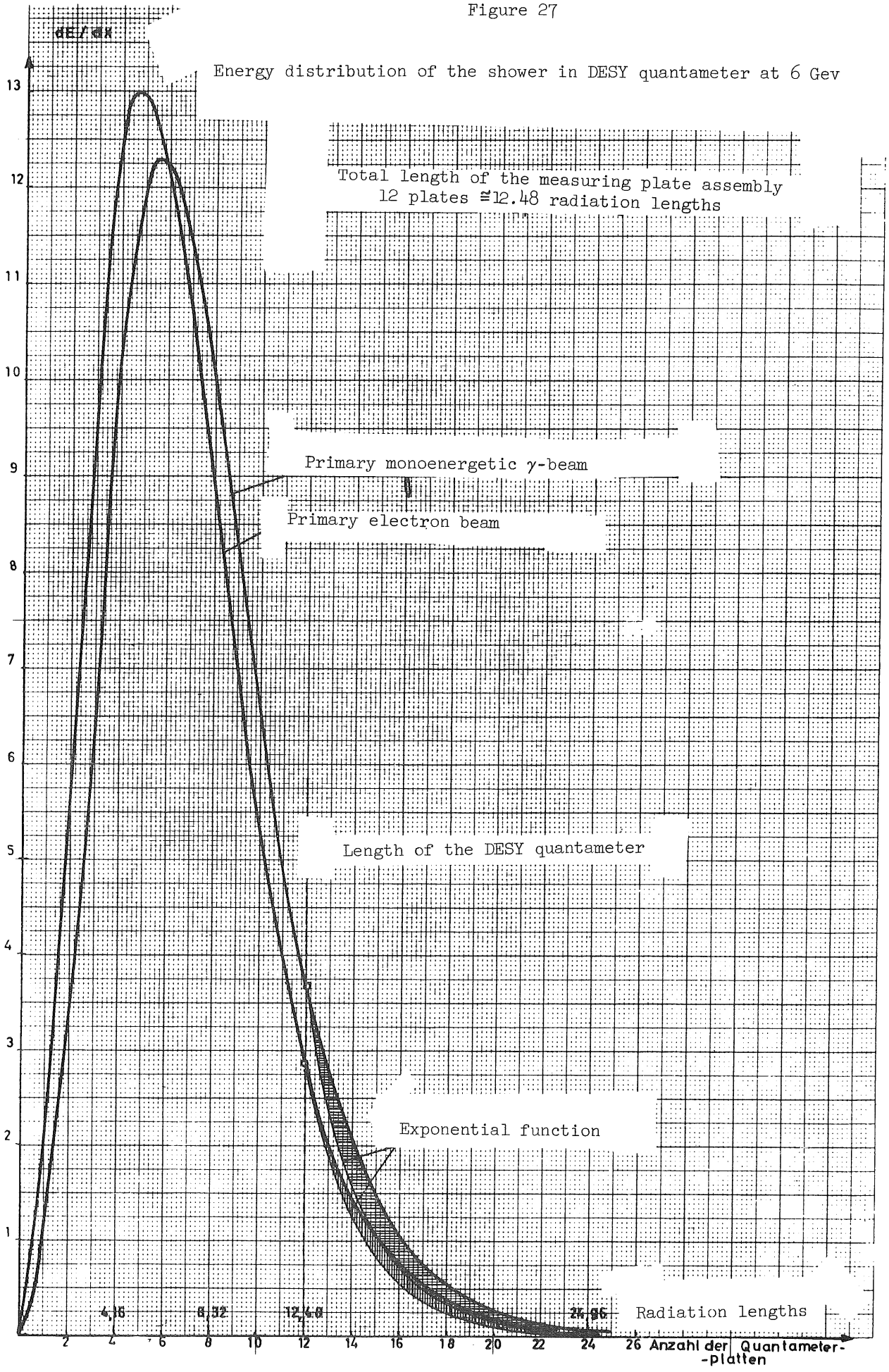

Number of plates in the quantameter

Figure 28

Time dependence of individual measured values during calibration of the gas-filled quantameter

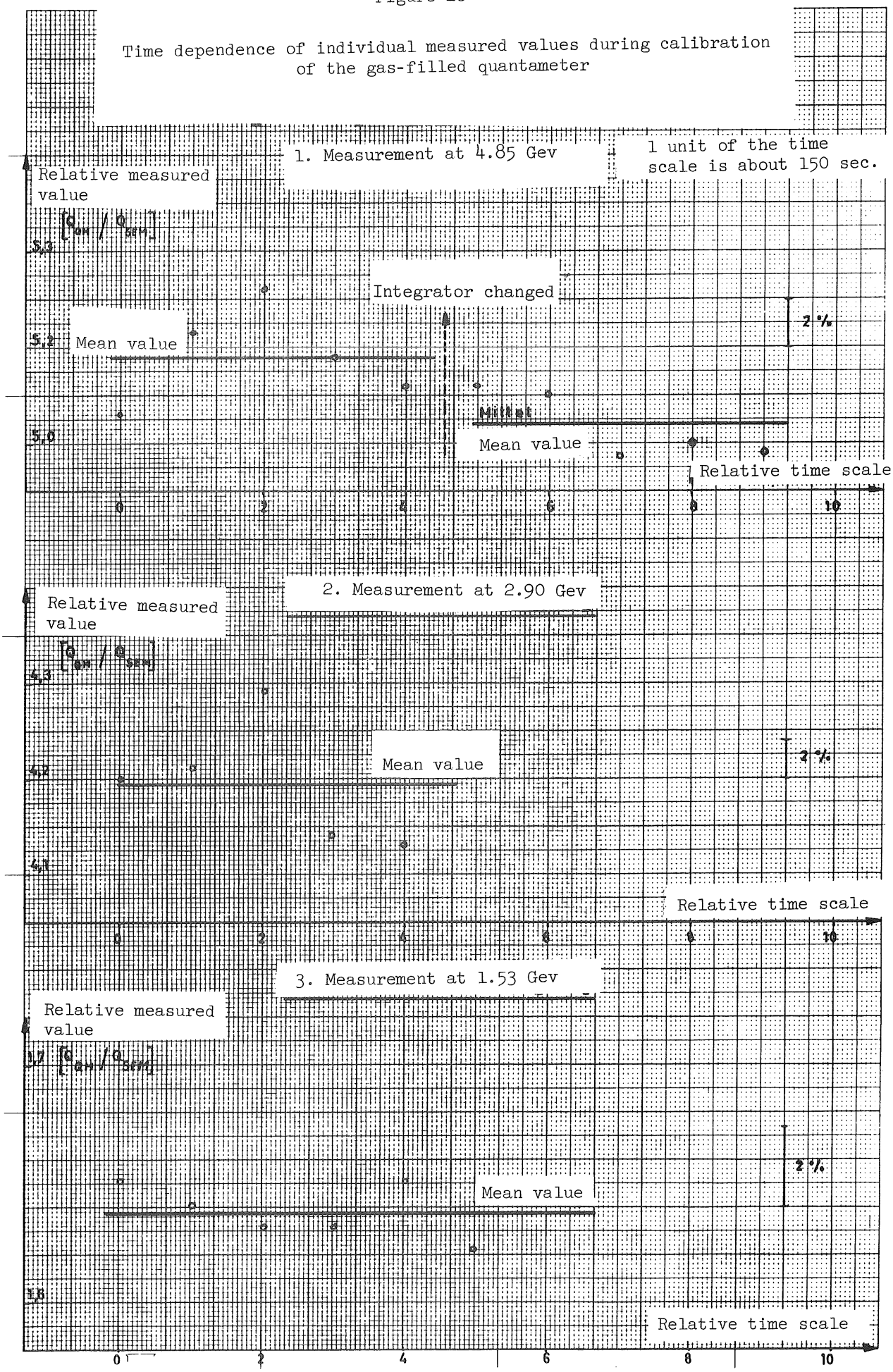

Figure 29

Measured values as a function of the beam shifting, for the secondary emission quantameter at 4.24 and 1.78 Gev

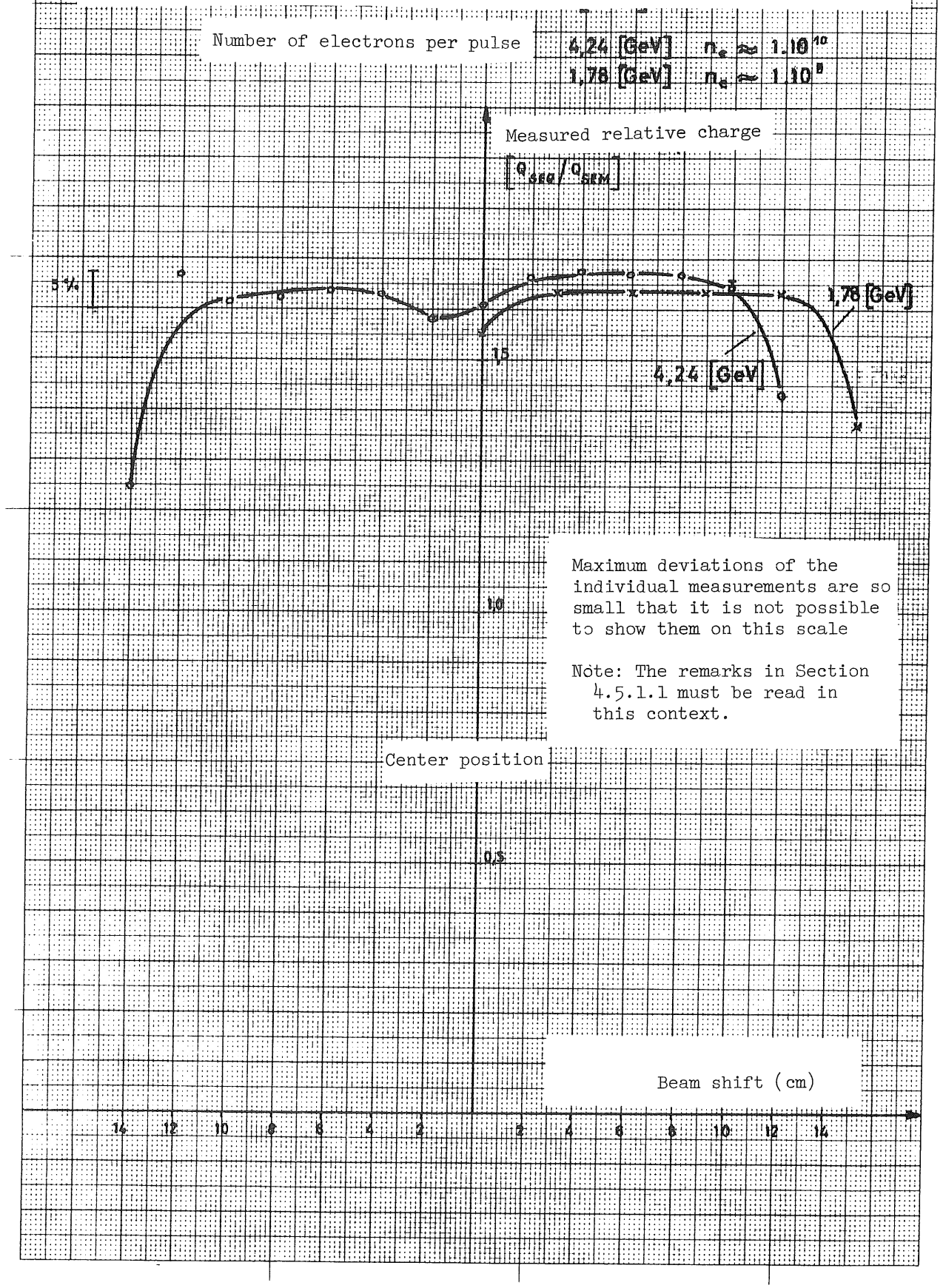

Figure 30

Current-voltage characteristics of the secondary-emission quantameter

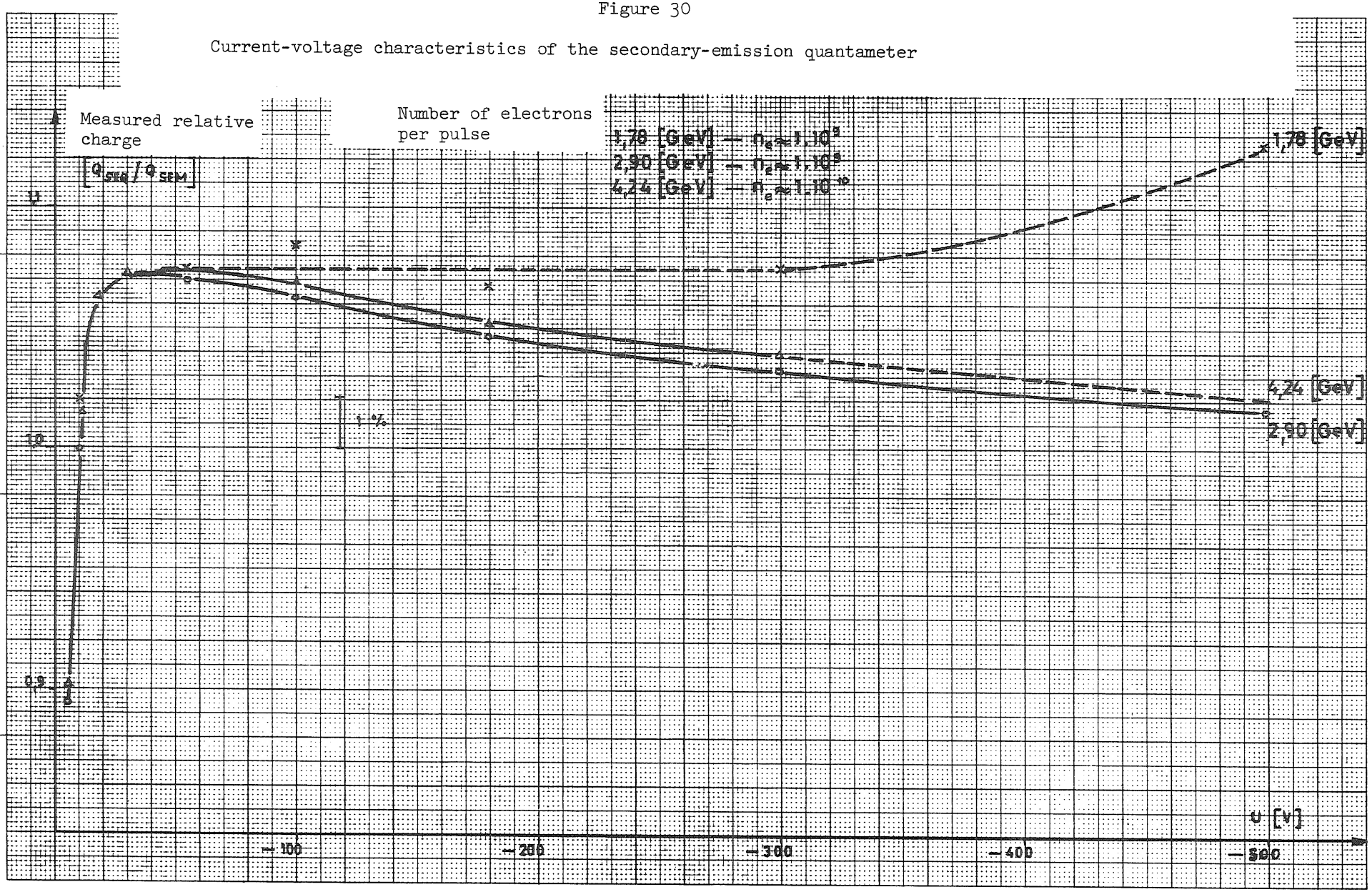

Figure 31

Current-voltage characteristics (plateau) of the secondary-emission quantameter

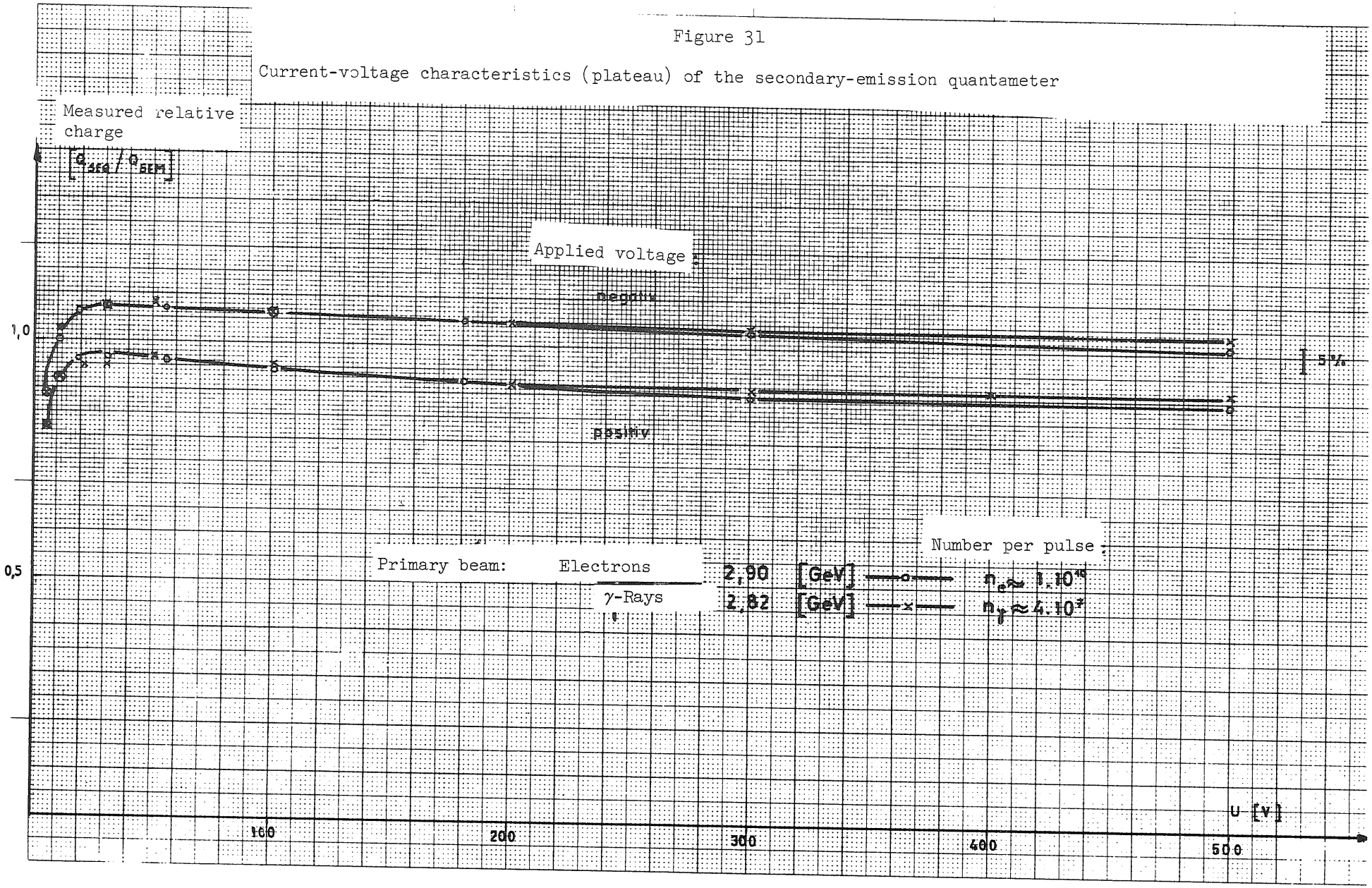

Figure 32

Energy dependence of the calibration constant of the secondary emission quantameter

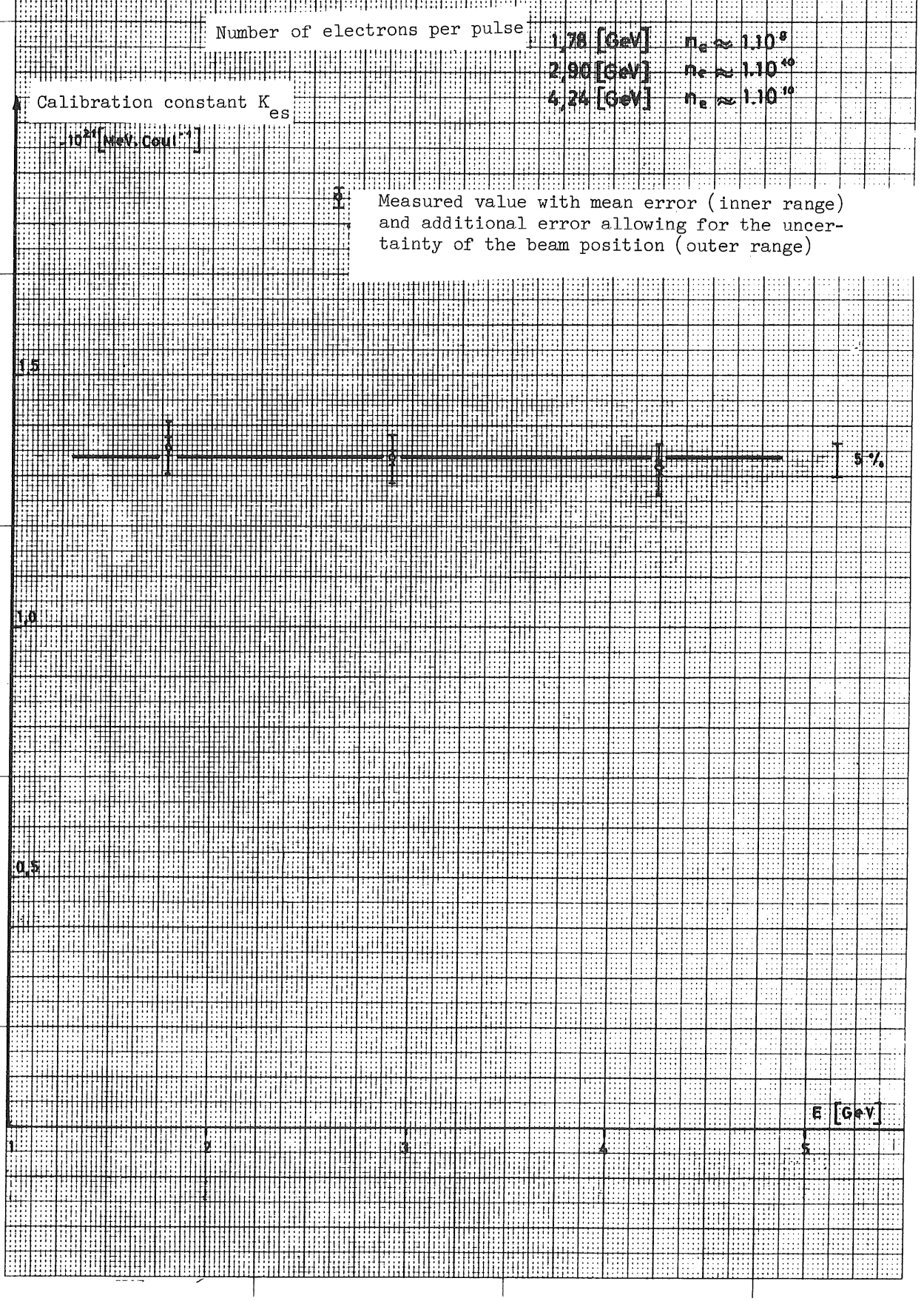

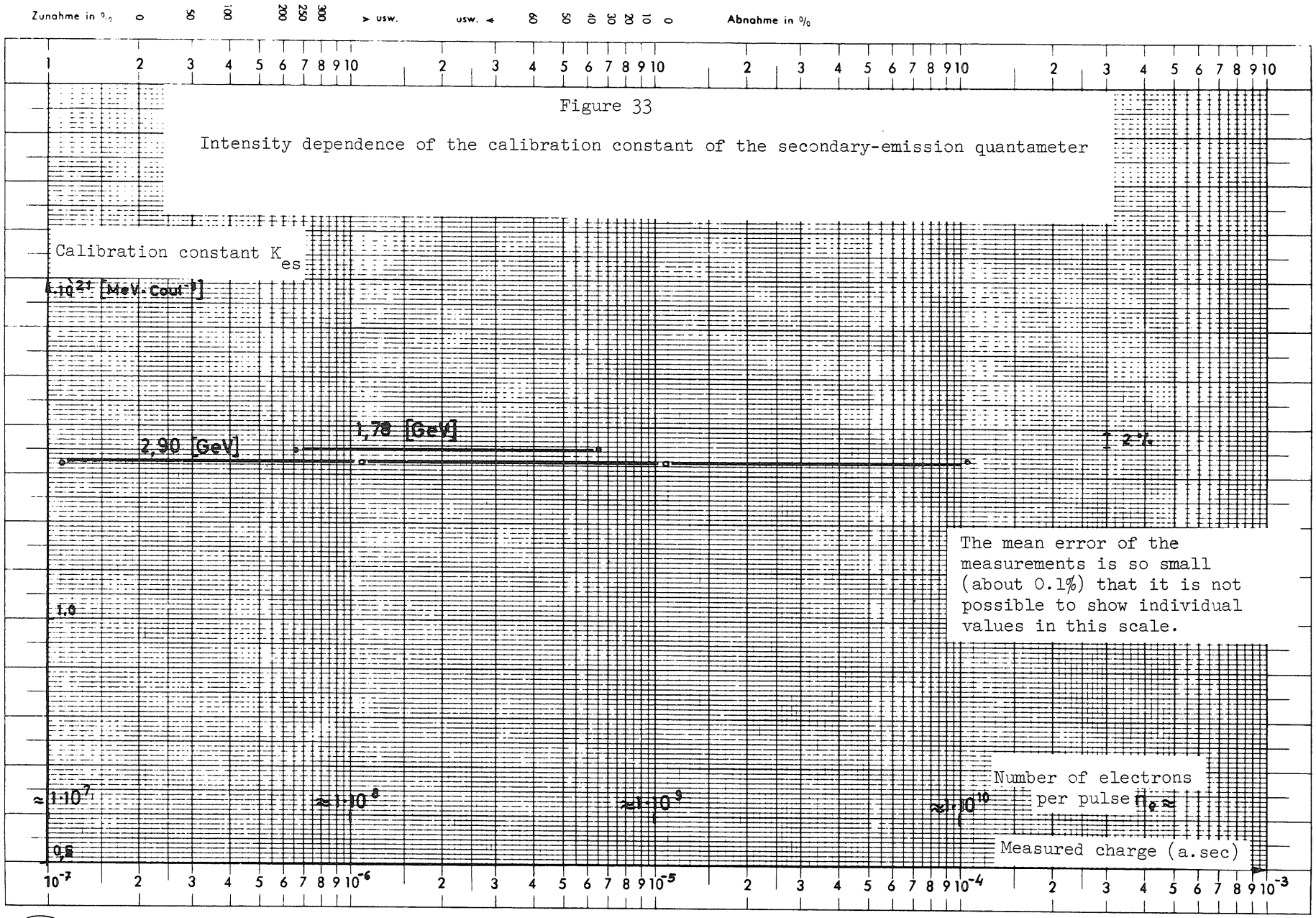

Figure 33

Intensity dependence of the calibration constant of the secondary-emission quantameter

Eine Achse logar. geteilt von 1 bis 10000, Einheit 62,5 mm, die andere in mm mit Prozentmaßstab

Figure 34

Time dependence of the measurements of the secondary emission quantameter calibration constant